CHALMERS

Air Target Measurement Accuracy In The Presence Of Ground Clutter

JOHAN ENGBLOM

Master Thesis
Department of Signals and Systems
Chalmers University of Technology
Göteborg, Sweden, 2009 EX090/2009

Foreword

This project and Master Thesis is primary done for Saab AB and in second hand for the institution of Signals and systems at Chalmers University of Technology. I would like to thank my tutor at Saab AB, Stefan Eriksson and all personnel at Saab AB who has been part of this project.

Abstract

Target tracking algorithms in radar systems have to operate in an environment of measurement uncertainty. A condition for good target tracking in a radar system is that a target position can be estimated and the measurement accuracy can be determined.

The main problem is that clutter cannot be well defined by a stationary stochastic process and there is no known general model that works in different clutter environments. A mobile radar system is often presumed to be able to function in various environments such as: Sea, littoral regions, mountainous terrain, flatland and deserts.

By using a target simulator with the actual radar system and a true clutter environment, a large amount of field data, is recorded during different system settings. These recordings are then used to estimate the systems measurement accuracy.

The result is a fine-tuned algorithm of the measurement accuracy. The algorithm is evaluated and compared to the current system implementation using a target in a real clutter environment. The proposed model is shown to improve the accuracy estimations by 7 times compared to the current model in the elevation coordinate. An improvement of 3 times could be identified in the azimuth coordinate.

Contents

1 Introduction

1.1 Background

Target tracking algorithms in radar systems have to operate in an environment of measurement uncertainty. A condition for good target tracking in a radar system is that a target position can be estimated and the measurement accuracy can be determined.

The target tracking filter (e.g. Kalman filter) typical weights a new measurement with a predicted value based on several previous measurements and physical criterions. In literature, accuracy relationships are based on the signal strength and a few known system parameters: Signal-To-Noise (SNR), a fixed random error and a bias error. Although, these basic relationships are only valid when measurements are performed in thermal noise and in absence of unwanted signals such as multipath reflections and clutter. In presence of clutter, position estimation tends to be erroneous which can cause large problems for the target tracking filter, such as track lost, track mismatch or tracking position error.

Clutter is defined as unwanted radar echoes, what is seen as clutter varies depending on the radar system surveillance objective. For a military air-surveillance radar objects with low speed is (in most cases) considered as clutter, i.e. birds, water, rain, etc. [1]

The main problem is that clutter cannot be well defined by a stationary stochastic process; the mean and the autocorrelation functions are invariant to a time or space shift [2]. A numerous of studies [3] has proven that site generic clutter models doesn't serve well in real situations and is therefore hard to validate. A mobile radar system must be able to function in various environments such as: Sea, littoral regions, mountainous terrain, flatland and deserts, it is therefore interesting to know how the accuracy is affected by clutter.

As described above the target detection gets more complicated when the target echo is mixed with clutter. A way of measuring the clutter associated to a specific target measurement is to use a constant false-alarm algorithm (CFAR), which typical uses the video levels in the surrounding cells of a target and compares the video level to a detection threshold to decrease the probability of false detections. The detection threshold is then a measurement of the reflectivity from the surrounding cells, thus, as this is unwanted signals these reflections are clutter.

1.2 Objective

By studying the measurement accuracy for single targets in the presence of ground clutter an algorithm is designed and evaluated. The expected result is a fine-tuned algorithm of the measurement accuracy which describes the accuracy for a target when thermal noise, random errors from the radar system and clutter is present.

A simplified block diagram of the signal processing and tracking is shown in Figure 1. For each target detected the signal processing extracts a set of estimated parameters: Range, Bearing, Elevation, Doppler, SNR, etc. Based on these parameters accuracy estimation is done and the value is passed to the Tracking block. The accuracy estimated should be accessible with as little computational cost as possible, as the system is working in real time.

Further on, a high performance radar system uses different system modes (settings) to achieve diversity and change radar target objective (i.e. what is important to detect) which changes the accuracy estimation. For example the antenna might change the number of revolutions per second, causing the accuracy estimation to change.

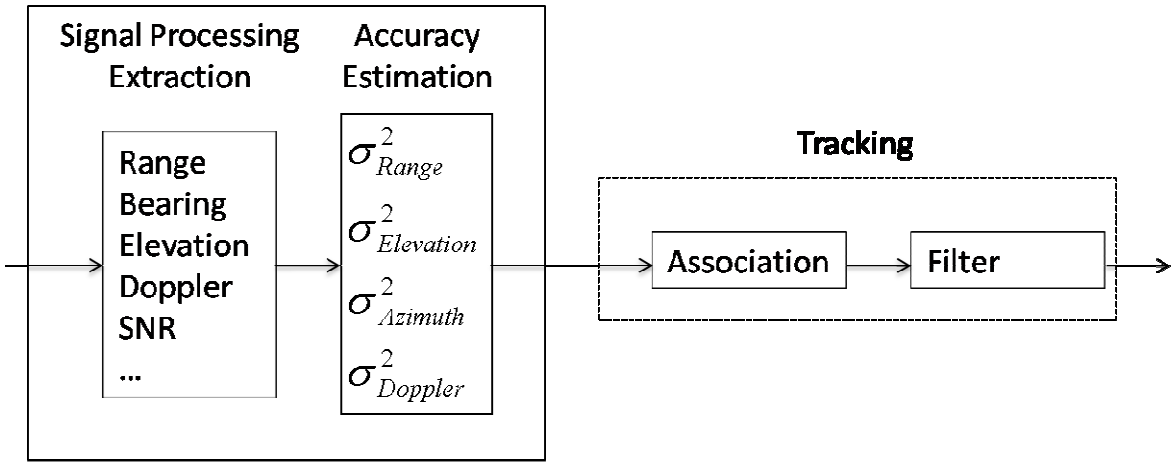

Figure 1 Block diagram showing where the accuracy estimation is position in a radar system.

Even though the tracking algorithm design is not part of the project it is important to understand how accuracy estimation is used. Picture yourself two targets, flying closely in parallel, if the target accuracy is defined very loosely for both targets the targets might get mixed. A problem also arises when the target accuracy are too high, while it should be set much lower. This might falsely force the tracker to assume the target has changed direction and loose the track. Also remember that tracking is done at real-time with a finite amount of memory and computation resources.

2 Theory/Method

2.1 Radar theory

2.1.1 A simplified radar system

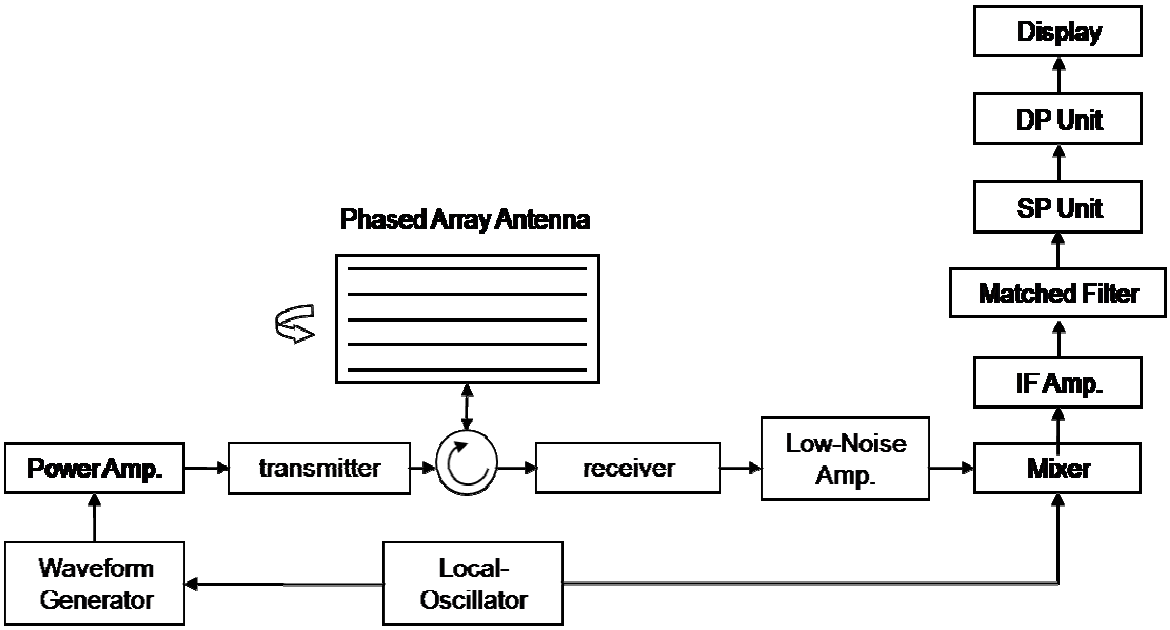

Figure 2 Simplified Radar system block diagram with a power amplifier and a receiver of superheterodyne type. SP Unit is in direct contact with SP Extractor in Figure 1.

A typical radar system can be simplified into Figure 2.

The duplexer acts as a switch to protect the receiver when the high power transmitter is on and redirects the signals to the receiver when the transmitter is off.

To achieve an azimuth perspective the antenna rotates, but to achieve a resolution in elevation angle, the radar either has to mechanical steer the antenna in elevation angle, use electronic steering or (digital) beam forming (DBF). The later is used in Saab Giraffe AMB®.

The receiver is typically of (super) heterodyne type, with a local oscillator (LO) the signal is mixed to an intermediate frequency which is convenient to process. Often the IF amplifier is combined with an approximation of the matched filter which maximizes the Signal-to-Noise-Ratio (SNR).

The signal processing unit or SP Unit in Figure 2 serves to remove undesired signals (clutter) and pass detections to the data processing unit. Doppler or a Moving Target Indication (MTI) filter, pulse compression and CFAR is also part of this block.

The data processing is depending on the application, but for an air surveillance application target tracking is one essential example but numerous other functions could be applied here. It is important for the target tracking function to only report desired targets.

In addition a radar control can be used that changes the radar system setup depending on the current objective for a radar operator. A modern radar system can change frequency, waveforms and different signal processing to maximize its performance in different environments.

2.1.2 Radar Principles

The basic radar principle is to transmit a high power pulse (radiate electromagnetic energy) which travels with the speed of light and wait to the pulse to be reflected from and returned to the receiver. The distance is given by the time Δt between transmit and receive times the velocity c of the wave in current medium divided by two as the pulse travels a round-trip path (1).

$$R = \frac{c\Delta t}{2} \tag{1}$$

If a target is moving between two measurements relatively the radar a shift in frequency in the receiving echo signal will occur, due to the Doppler Effect [4]. The Doppler frequency (2) is given by the velocity and wavelength λ.

$$f_d = -\frac{2v}{\lambda} \tag{2}$$

The transmitter of a typical Ground-based air-surveillance system such as Saab Giraffe AMB® (Agile Multiple Beam) uses a Travelling Wave Tube (TWT) which has high output power which is required when long range coverage is the objective. [4].

The radar range equation [4] is for a monostatic radar. Monostatic radar systems use one antenna for both transmitting and receiving. Increasing the radar range with factor two implies a 16 times higher average transmitting power; this can be derived from the radar range equation (3).

$$P_r = \frac{P_t G_t \sigma \cdot F}{(4\pi)^2 R^4} \cdot A_e \tag{3}$$

Where P_r is the receiving power, P_t is the transmitting power, G_t the transmitting antenna gain, σ is the reflectivity of the target, F is the pattering propagation factor, A_e effective aperture of the receiving antenna, R is the distance from the antenna to the target.

Pulse Repetition Frequency is how often a pulse is repeated, the choice of PRF is crucial as it effects to what extent ground and moving clutter can be rejected. It also determines what the range and Doppler ambiguous will be. [5]

The number of pulse echoes received by the radar is a function of the beamwidth, Pulse repetition frequency (PRF) and the rate of the antenna rotation:

$$N_\theta = f_s t_d = f_s \frac{\theta}{\omega_a} \tag{4}$$

Where the number of pulse echoes received (N_θ), f_s is the PRF in Hz and t_d is the dwell time on the target in seconds, θ is the beamwidth in radians and ω_a is the antenna rotation in radians per second.

The antenna beamwidth, θ_{3dB} is related to the antenna size ω, k_A and radar wavelength by [6]:

$$\theta = \frac{k_A \lambda}{\omega} \tag{5}$$

The 3 dB beamwidth or half power beamwidth is usually calculated in azimuth and elevation plane. The effective aperture area tells us what the received power is for the antenna and is given by:

$$A = \frac{G\lambda^2}{4\pi} \tag{6}$$

Where, G is the gain of the antenna.

The antenna beamwidth determines the angular resolution, i.e. the smaller beamwidth the higher the resolution. The antenna always has side-lobes; low side-lobes are often desired as they allow viewing of targets that are close together. To reduce the side-lobe levels a method called aperture illumination (also called taperin or weighting) is used, which aims at lower the current density near the edges of the antenna. The price you have to pay is antenna efficiency, reduction in gain and increased bandwidth. [6]

As a rule of thumb the side-lobe mean power level relative to the antenna main beam should be with N antenna elements: 1/N. E.g. for a antenna with 20 elements the side-lobe levels is ~-26dB.

Polarization is defined as: “The direction of the electric field vector is aligned during a passage of at least one full cycle” or in which direction the oscillation occurs. The polarization properties of the transmitted signal can be vertical, horizontal, elliptical and circular which gives different properties. Based on the objective of the radar the polarization property selected should diverge from the target properties as far as possible. E.g. A radar with perfect circular polarization has perfect clutter rejection for perfect symmetrical raindrops, thus, weather radar should not have circular polarization. Often a combination of different polarization properties are used to increase the clutter rejection, two receiving antennas could be used simultaneous with different polarization properties.

2.1.2.1 Phase Array Antenna

When a lot of targets are needed to be observed at the same time phase array antennas is useful. The beams can be electronically scanned instantly, only limited by the computer power available. As of the last decades increase in computation power this alternative is very attractive.

A typical phase array antenna is the type shown in Figure 2, where the rectangular antenna elements are stacked vertical. As a target echo reaches one antenna element at different time than another antenna element, the minimum bandwidth can be calculated as:

$$B_A = \frac{c}{\omega \sin\varphi} \tag{7}$$

Where φ is the beam elevation or azimuth angle

The distance between two antenna elements is around λ/2, for C-band (~5.4GHz) radar the total height of an antenna with 20 elements is approximately 0.5 meter. As the distance between the two antennas elements will cause the signal to appear at different times in the antenna elements, to create a single beam a small time delay is introduced, this time delay is equivalent to a phase shift when the bandwidth is only a fraction of the centre frequency (5.4 GHz versus 1 MHz) and such antennas is therefore called phase array antennas. [7].

2.1.2.1.1 Digital Beam Forming – DBF

The digital beam forming (DBF) is the concept of combining different input signals and forming lobes, a kind of Multiple Input Multiple Output structure. When transmitting a pattern the beam is created by using constructive and destructive interference. When receiving each antenna element signal is combined according to a predefined filter or structure. The concept is illustrated in Figure 3, the filter is defined as the constants a_{ij}, which will form the beams.

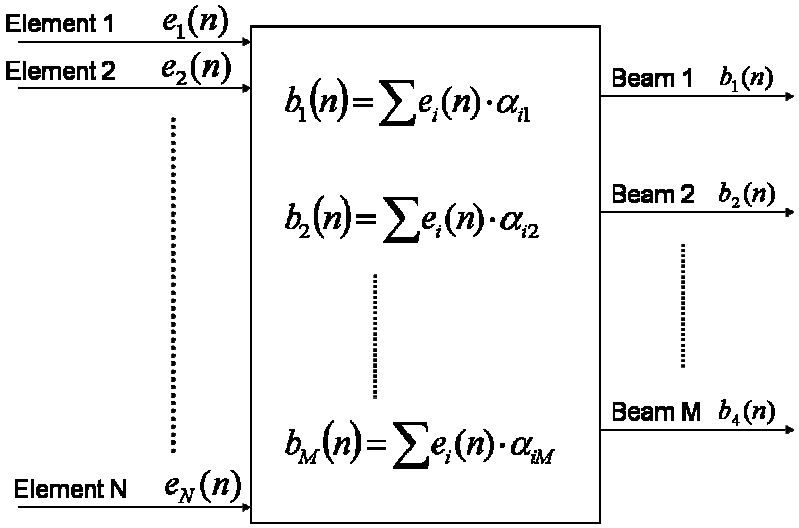

Figure 3 Digital beam forming, the elements are combined with constants (a_{ij}) representing a weighting function.

2.1.3 Signal Processing

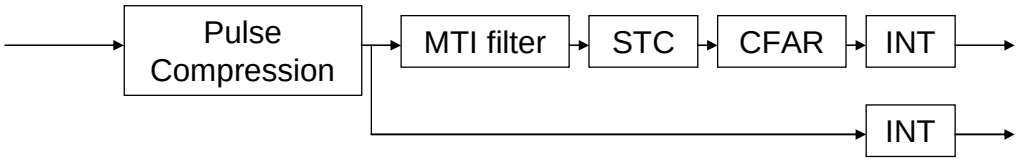

Figure 4 Signal Processing Block Scheme

2.1.3.1 Pulse Compression

Pulse compression combines high output energy with good range resolution, it is used to find the signal pulses, i.e. by a match filter. An ideal match filter is the filter that maximizes the SNR. Decoding of the signal is also done here, the signal could be modulated in any kind of signal modulation scheme. Binary-Phase-Shift-Keying (BPSK), where the signal is phase shifted 180°. Typical signal values is minus one and one. The last step is to pass the received pulses through a filter whose time-frequency characteristic is the conjugate of the coding. [5]

2.1.3.2 Moving Target Indication

The purpose of the Moving Target Indication (MTI) filter is to remove unwanted signals that are originating from stationary slow-moving targets, while remaining fast-moving objects. The MTI filter uses the Doppler frequency to distinguish the velocity of a target by sending several pulses in an interval, i.e. Pulse Repetition Interval (PRI).

A typical MTI filter with rain and clutter rejection is visualized in Figure 5.

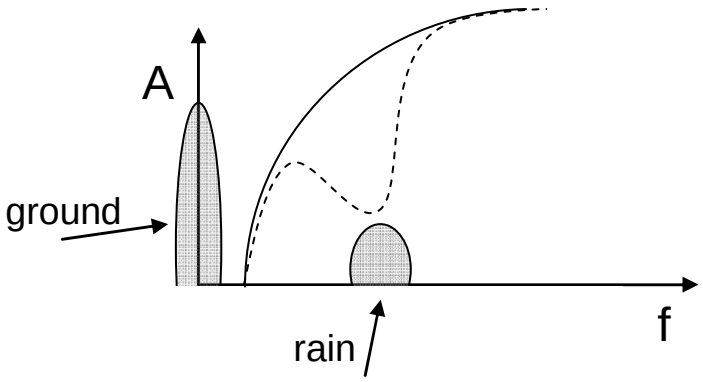

Figure 5 MTI filter, after rain an clutter rejection dotted

2.1.3.3 Sensitivity Time Control

To limit strong returns from ground clutter very close to the radar the 4th root relation from (3) is used in the radar system signal processing, if this method would not be used the radar system would be saturated and thus be blinded by this echoes.

2.1.3.4 False Alarm Control

If fixed detection thresholds are use, in the presence of clutter this will lead to an enormous number of detections. A solution is to set a sufficient high global level, so the number of false detections is reduced, thus this solution would reduce the target sensitivity and is not realistic in high performance air surveillance radar. One technique to approach this problem is adaptive thresholding. Adaptive thresholding uses the surrounding cells of the supposed target detection to estimate the threshold, shown in Figure 6. As visualized the target sensitivity is lowered, therefore the design of the CFAR filter is critical. The CFAR filter design parameters is: level, filter length and calculation method. Example: Setting a too high level will result in low target sensitivity (CFAR loss) while setting the filter length very short would result in higher sensitivity and thus result in higher probability of false detections.

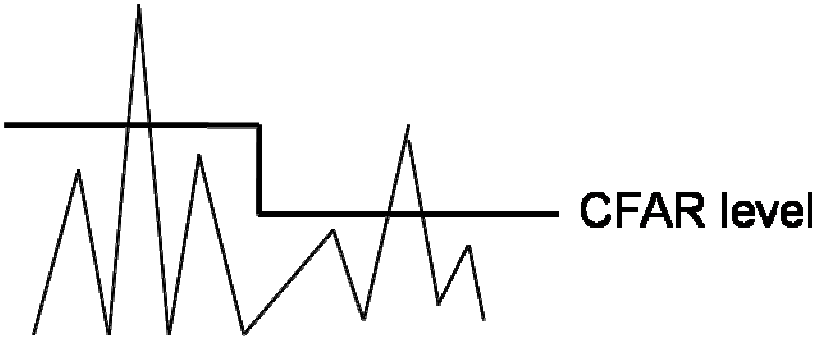

Figure 6 Adaptive threshold concept.

I.e. the CFAR algorithm finds the magnitude of the echoes in adjacent cells and computes the logarithmic sum and sets a threshold.

2.1.3.5 Integrator

An integrator is used to maximize the SNR by matching a filter to the number of pulses illuminating a target during each antenna scan. find the level before detection; the integrator uses a matched filter in bearing, matched to azimuth beamshape to avoid multiple detections.

2.1.4 Measurement Accuracy

2.1.4.1 Range

The range is calculated as the time between transmit and receive times the velocity of the wave in current medium divided by two as the pulse travels a round-trip path (1). The range-measurement accuracy (8) is characterized by the rms measurement error, σ_R, given byt the root-sum-square three error components. [6]

$$\sigma_R = \sqrt{\sigma_{RN}^2 + \sigma_{RF}^2 + \sigma_{RB}^2} \tag{8}$$

Where,

- σ_{RN} is the SNR dependent random range measurement error
- σ_{RF} fixed random error including the range error from propagation due to multipath conditions.
- σ_{RB} is the bias error component.

The thermal noise dependent radar range error usually dominates the range error and the standard deviation is described by:

$$\sigma_{RN} = \frac{\Delta R}{\sqrt{2SNR_{dB}}} \tag{9}$$

For a radar system with a 50 m range gate (ΔR), the thermal noise dependent error is 11 m at 10 dB and 5 m at 55 dB using equation above. But for higher SNR the fixed random error, σ_{RF} usually limits the radar performance as the radar internal noise is typical at 25-30 dB [6], which results in random fixed errors of $1/25^{th}$ to $1/80^{th}$ of the range resolution, which is two meters to 0.5 meters for the example above.

The bias term is largely dependent on how much care is taken to resolve this issue, and is therefore highly system dependent. The range bias can be from a few meters up to several hundreds of meters all depending on the system objective. For a air target tracking system where the radar the absolute position is important, calibration is often used to limit the bias error to be in proportion to the fixed random error.

2.1.4.2 Velocity

The velocity is measured from the Doppler frequency shift of the received signal; the Doppler frequency is given by (2). Radial velocity measurement accuracy, σ_V is characterized by the root-sum-square three error components:

$$\sigma_V = \sqrt{\sigma_{VN}^2 + \sigma_{VF}^2 + \sigma_{VB}^2} \tag{10}$$

Where,

- σ_{VN} is the SNR dependent random radial-velocity measurement error
- σ_{VF} fixed random error including the range error from propagation due to multipath conditions.

- σ_{VB} is the radial-velocity bias error component.

The thermal noise dependent error usually dominates the error component, the standard deviation is described by (11), where τ is the pulse-length.

$$\sigma_{VN} = \frac{\lambda}{2\tau\sqrt{2SNR_{dB}}} \tag{11}$$

The fixed random error limits the performance in high amplitudes and the bias terms are usually very small in absence of multipath conditions. The bias term is usually calibrated to be in proportion to the fixed random error.

2.1.4.3 Angular

The radar angular measurements described use monopulse receive antennas that have simultaneous receive beams offset in angle to either side of the transmit beam. The difference pattern formed by these beams may be used to measure target angular position with a single signal transmission.

The measurement accuracy in each angular coordinate is characterized by the rms measurement error, $\sigma_{A,}$ given by the root-sum-square three error components: [6]

$$\sigma_A = \sqrt{\sigma_{AN}^2 + \sigma_{AF}^2 + \sigma_{AB}^2} \tag{12}$$

Where,

- σ_{AN} is SNR dependent random angular measurement error and is the dominating source of error.

- σ_{AF} is a fixed random error from the propagation and radar random error. The fixed angular random errors will limit the radar performance in higher SNR values.

- σ_{AB} is the angle bias error, which in most cases will be small.

The thermal noise dependent angular error is given by:

$$\sigma_{AN} = \frac{\theta}{k_m\sqrt{2SNR_{dB}}} \tag{13}$$

Where θ is the 3dB-beamwidth and k_m is the monopulse pattern difference slope [6]. The value of k_m is usually 1.6 [8].

In addition the accuracy has to be corrected as the accuracy relationship derived above is for a monopulse radar and Giraffe AMB uses different system modes and uses signal processing techniques which are not ideal, i.e. the matched filter and MTI filter.

2.2 Radar clutter

Radar clutter is defined as unwanted echoes, typically from the ground, sea, rain etc. What is seen as clutter depends on the radar system purpose. For a tracking radar system; most low-speed objects are seen as clutter, e.g. land, buildings, rain and birds.

Two simple classifications of clutter can be made: Volume such as rain and chaff (a radar countermeasure method which uses metal foil to decoy the radar), and surface such as ground and sea. In this project only ground clutter will be directed, but it is important to understand the difference between the clutter types and what is seen as ground clutter.

2.2.1 Volume clutter

Volume clutter ex. Rain and Chaff, are more homogeneous in spatial distribution and more nearly noise-like than other clutter types [1].

$$V_c = \frac{R_c \theta_a}{L_p} \frac{R_c \theta_e}{L_p} \frac{\tau_n c}{2} \tag{14}$$

Volume clutter is given by (14), where V_c is the clutter volume, R_c is the clutter range and θ_a and θ_e are azimuth and elevation beamwidths in radians, L_p = 1.33 is the beamshape loss, τ_n s the width of the processed pulse and c is the speed of light. The radar cross section (RCS) filling this volume is

$$\sigma_c = V_c \eta_v$$

, where η_v is the volume clutter reflectivity.

2.2.2 Surface clutter

Surface clutter is extremely difficult to model, so mathematical models are idealized [4]. Nature and man-made objects are inhomogeneous from a radar perspective, as well as the propagation and scattering changes depending on the current weather condition, e.g. windy conditions would lead to heavy clutter. Also, different moisture levels on the ground could lead to different clutter characteristics. A classification of all objects would result in an infinite amount of classes. To perform an analysis, the world has to be simplified. Therefore all models are more or less deviating from the true clutter environment.

Radar ground return is most easily described by σ^0, which is the differential scattering cross section or scattering coefficient. The illuminated ground area depends on radar parameters such as pulse width, beamwidth etc as illustrated in Figure 7.

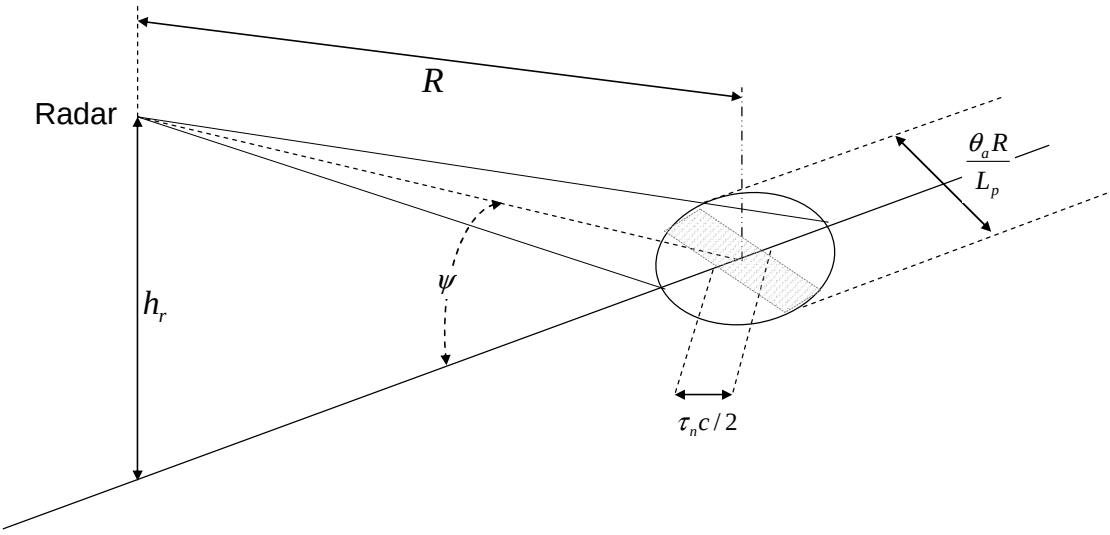

Figure 7 Geometry of surface clutter, where θ_a is the azimuth beamwidth, τ_n is the width of the processed pulse after pulse compression, $\sec\psi$ is one for surface based radars (using small angle assumption), L_p is the beamshape loss and c is the speed of light.

The area of surface within the radar resolution cell is:

$$A_c = \frac{R\theta_a}{L_p}\frac{\tau_n c}{2}\sec\psi \tag{15}$$

Where, A_c is the geographical area presented in Figure 7. Notice that (15) describes the ground surface area and not the projected area.

The Radar cross section for a geographical area or the area of the reflected pulse is described by:

$$\sigma_c = A_c\sigma^0 = \gamma\frac{h_r\theta_a}{L_p}\frac{\tau_n c}{2} \tag{16}$$

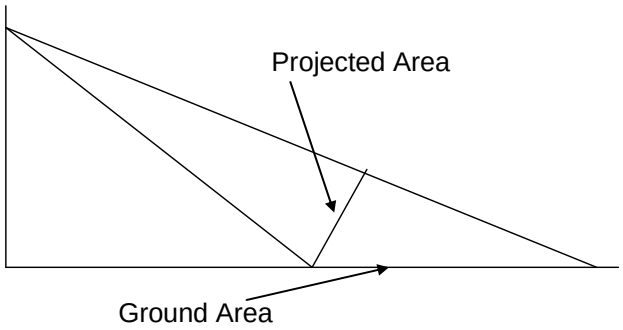

Figure 8 Difference between ground (geographic) and projected area

The echoes resulting from ground clutter may be large in both areal size and intensity. The effects of ground clutter fall off as range increases usually due to the curvature of the earth and the tilt of the antenna above the horizon.

2.3 Measurement error estimation

2.3.1 Model

The total measurement error (17) is described by three error components, SNR which is the amplitude relation to thermal noise, STR which is the reflectivity of the surroundings cells of a detection, extracted by the CFAR algorithm. Outlier errors or non-linear errors are those errors that can't be described by a model. For example a radar system design could affect the error in either positive or negative direction in different system settings or not be prominent at all.

$$\hat{e}_{tot} = \hat{e}_{SNR} + \hat{e}_{STR} + \hat{e}_{outlier} \tag{17}$$

2.3.2 Curve fitting

Current accuracy model for Giraffe AMB uses an exponential decay curve derived from (13). Therefore it is a good starting point to assume that the accuracy will follow this model. Although, $\forall x_i's$ free to take any real value. The function f (18) is the standard deviation or standard error as a function of SNR, the function is derived from both on experiments and theory (13).

$$f(SNR_{dB}) = x_1 + \frac{x_2}{10^{(x_3 \cdot SNR_{dB}/10)}} \tag{18}$$

We could view x_1 as the estimation of the fixed angular error (σ_{AF}) which will limit the radar performance for detections with higher SNR.

The Least-Squares method is used to fit the data towards the model by minimising the residual sum of squares:

$$\begin{aligned} x &= \begin{bmatrix} x_1 & x_2 & x_3 \end{bmatrix} \\ A \cdot x &= B \\ x &= A^{-1}B \end{aligned} \tag{19}$$

Where *A* is SNR_{dB} and *B* is the residual squared.

(19) calls for a linearization of (18), but direct linearization cannot be performed as this will create an intrinsically nonlinear parameter estimation problem. Either a parameter must be fixed or nonlinear regression has to be used, as it is expected that the result from the regression should be close to the theoretical result linear regression is used.

In this project x_3 will be constant set to one and the least-squares method is performed at the other parameters, this will add an error in the Least-square regression analysis but the parameter can instead be used for real-time adjustment and correction, when required.

The linear regression is made on root mean square error in elevation and azimuth. For both parameters the linear regression is first made as a function of SNR, the residual is then used to regress the parameters as a function of STR. In elevation coordinate, the regression is divided into several elevation intervals.

3 Measurements

3.1 Procedure

To determine where the radar system detects clutter and strength of clutter a set of radar video recordings are done at the measurement site, the recordings are then processed to determine where high clutter amplitude is found. The recordings are made with the same radar system as the accuracy should be defined for (Giraffe AMB). The result of these opening measurements is a clutter map [1]that covers the whole geographical area that is seen by the radar system.

Measurements are performed with the use of a target simulator. Simulated targets are position in those areas where the clutter strength is high which was detected by the radar video recordings (see above). The target simulator injects echoes into the radar system that are a close approximation of true target statistics such as fluctuations in amplitude, velocity and azimuth angle. The simulator is designed to constrain the radar system to determine any difference between true targets and simulated targets, they are therefore treated the same way.

As the simulated target position is known (U_{true}) and the measured position ($U_{measured}$) is recorded from the radar system, a description of how the measurement error (20) depends on certain parameters can be done.

$$\varepsilon = U_{measured} - U_{true} \tag{20}$$

3.2 Clutter map

As we need to know where the radar detects clutter and the clutter strength, radar video recordings are made at the measurement site Saab AB. Radar video in this context is the Taylor tapered and phase shifted signal after DBF. The video contains azimuth, distance and the clutter strength divided into two channels: in-phase (I) and quadrature (Q). The recordings are made solidly in the lowest elevation beam pointing angle, as the highest clutter strength originates from ground reflectivity and backscattering.

A clutter map can be estimated using a classical Clutter map estimator [9] which averages over clutter values from different revolutions which are within the specific clutter cell area. Each cell covers a region of 0.7 degrees in azimuth and 48 m in distance. In the clutter map estimator (21): R is the current revolution within the clutter cell region defined by *i* and *j*. V is the clutter map for a single cell defined by *m* and *n*.

$$V(m,n) = \frac{1}{N}\sum R_1(i_1, j_1) + R_2(i_2, j_2) + ... + R_N(i_N, j_N) \tag{21}$$

$$Dist(m) - \frac{\Delta_{Dist}}{2} \le Dist(i_i) < Dist(m) + \frac{\Delta_{Dist}}{2}$$

$$Az(m) - \frac{\Delta_{Az}}{2} \le Az(j_i) < Az(m) + \frac{\Delta_{Az}}{2}$$

[1] The clutter map in this context is not related to the clutter map that exists in the Giraffe AMB radar system during operation.

The recordings are made in three different TX-modes: A binary phase shift (BPSK) pulse code with fast frequency change (FFC) (TX-mode A), a BPSK pulse code with slow frequency change (TX-mode B) and a short pulse mode with (FFC) (TX-mode C). For the BPSK modulated signals the pulse code is kept fixed to ease processing of the recordings. The pulse code is constant to ease the pulse compression, which is done at a PC. For each set at least 12 revolutions are recorded and a mean value is created within each clutter cell, the recordings are summarized in Table 1.

Table 1. Video recordings.

Revolutions	TX-mode	Frequency change	Pulse code
12	A	Automatic	Fix
12	A	Fix	Fix
12	B	Automatic	Fix
12	B	Fix	Fix
12	C	Automatic	Fix
12	C	Fix	Fix

A Clutter-to-Noise ratio (CNR[2]) is then calculated, the result is shown in Figure 9, Figure 10 and Figure 11. In Figure1 the recorded video for TX-mode 33 with FFC is shown, notice how the clutter is geographical spread in FFC mode compared to the SFC mode (TX-mode 42) with more scattering.

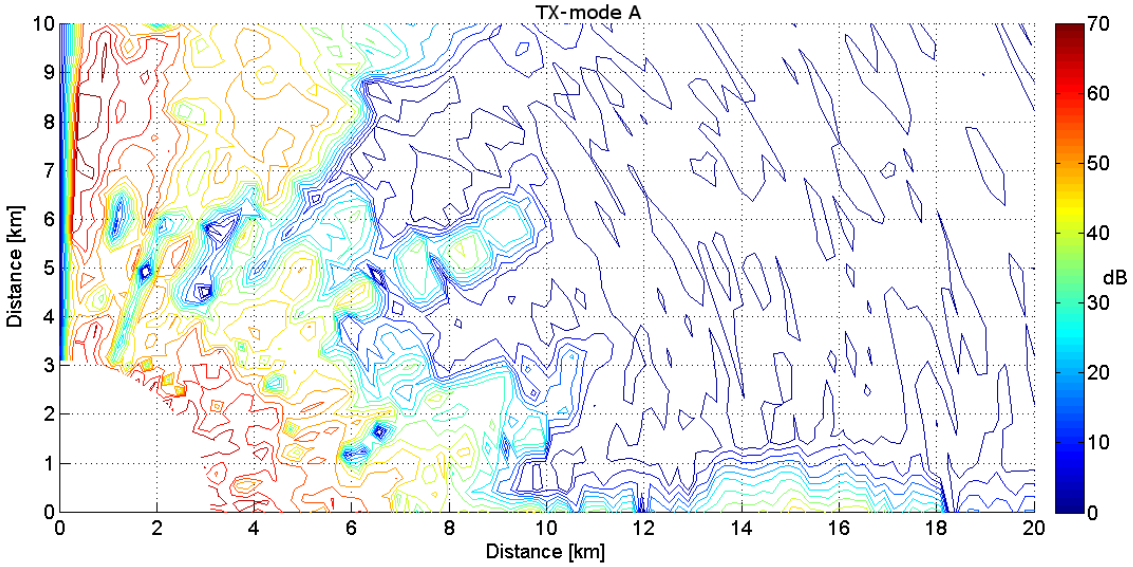

Figure 9 CNR for TX-mode A with FFC and BPSK modulation in the first quadrant [0º, 90º], the amplitude in dB [0, 70] shown in the pile.

[2] CNR is in this context Clutter-To-Noise Ratio

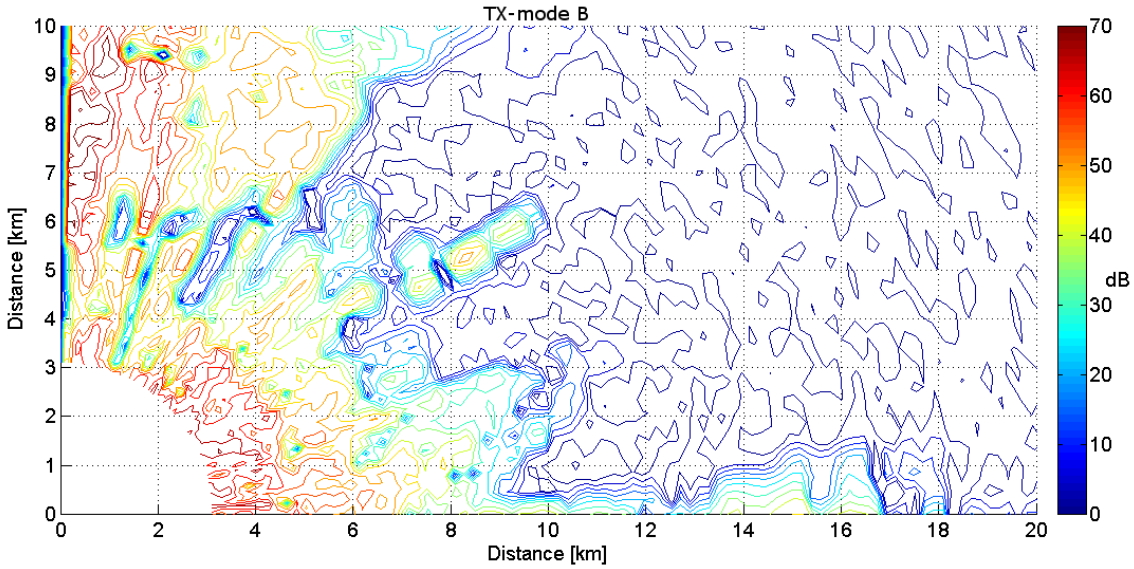

Figure 10 CNR for TX-mode B with SFC and BPSK modulation in the first quadrant [0º, 90º], the amplitude in dB [0, 70] is shown in the sidebar.

The CNR maps from TX-mode A and B are then combined according to (21), each TX-mode CNR map is treated as one revolution to weight the different recordings equally. The CNR map derived is shown in Figure 11 along with the max and mean value for a distance over 360º and the value of the dotted line at 73º in CNR.

Ground reflectivity tends to decrease with increasing range because of the curvature of the earth and the current topography. At long distances the earth's curvature causes the radar signal to propagate in free-space, this can be interrupted in mountainous or hilly terrain which can be seen in Figure 11 for the 73º line which drops to noise level as the radar signal is propagated through free space at 12 km distance but receives echoes again at 18 km.

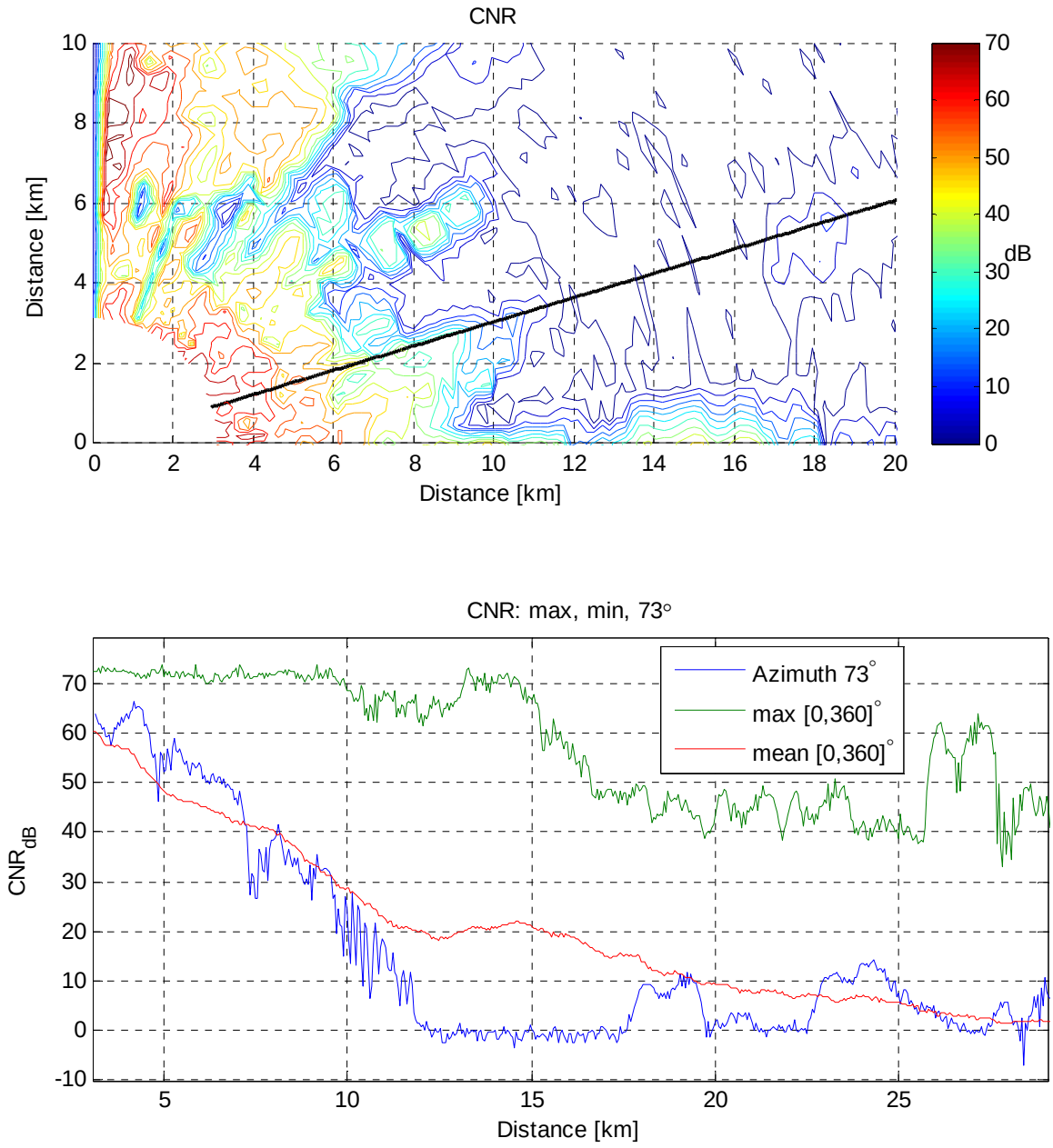

Figure 11 Above: CNR derived for TX-mode B with SFC and BPSK modulation and TX-mode A with FFC and BPSK modulation in the first quadrant [0º, 90º], the amplitude in dB [0, 70] shown in the pile. Below: CNR max and mean value for [0º, 360º] and CNR for the dotted line in above plot (~73º azimuth). The deep dip in the end of the transmission is caused by pulse decompression and should be neglected.

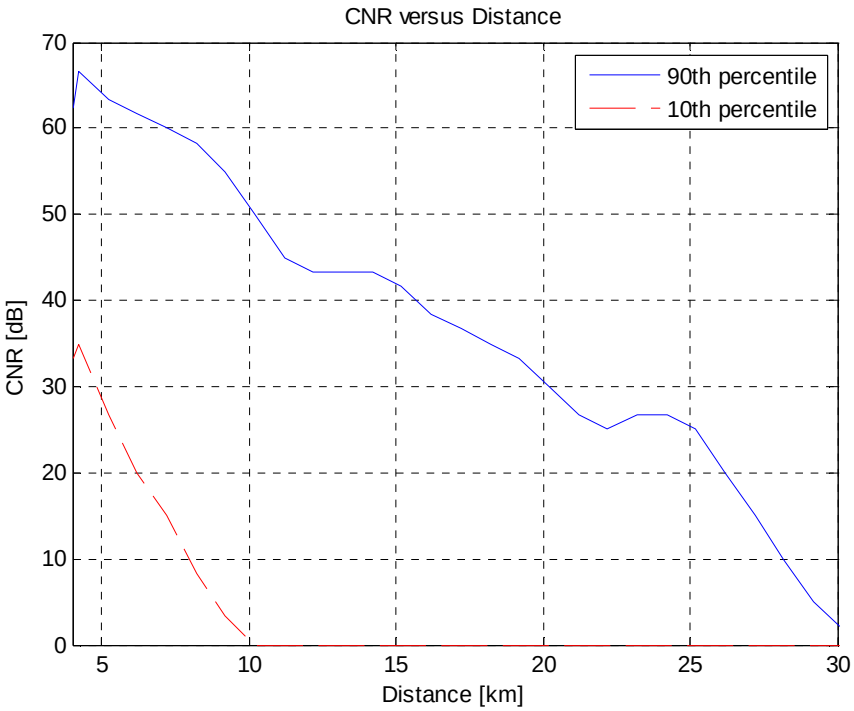

Figure 12 90 % and 10 % of the values are higher than specified CNR in current range gate, the gates are uniform at 1 km for 360 degrees azimuth.

The clutter levels are discretized into a uniform interval from 0 to 70 dB with 5 dB distance. The distribution of the clutter amplitudes are shown in Figure 12. As can be seen from the picture, high clutter amplitudes are easiest to find close to the radar, at ranges approaching 30 km the clutter amplitudes are decaying. E.g. 90 % of the values are higher than 65 dB at 5 km distance, while 90 % of the values are higher than only 3 dB at 30 km distance. As a reference the dotted 10 % line shows that 10 % of the values are lower than 0 dB after 10 km.

3.3 Simulated targets

From Figure 12 it is clear that a large amount of clutter cells contains amplitude levels at zero decibels. Therefore, it is not optimal to randomly generate targets over the whole volume, instead targets are positioned over those cell areas where the clutter level is within a specific interval, each target has then a specific CNR assigned. Although it should be mentioned that this value cannot be applied in the analysis for two reasons: The radar has a higher dynamic in bearing and the radar system calculates an own clutter strength value calculated in real-time based on the surrounding clutter levels as measured with the CFAR algorithm.

3.3.1 Target model

The simulated targets are fluctuating with a Swerling Case 1 model [1], which is a close approximation and widely accepted model of how a real fixed wing moving target fluctuates. The amplitude fluctuation is Rayleigh distributed and the phase fluctuation is uniform distributed. A new random value is generated for each new PRI if the current transmit frequency has not been used for the current target.

The target velocity must be fast enough so that the MTI filter doesn't suppress the target as clutter and slower than ambiguous velocity. As the MTI filter is altering in different tx-modes, the target velocity is set to 22 m/s, which is a velocity where different MTI-filters in the radar system don't reject the target as clutter.

3.3.2 Limitations

3.3.2.1 Range

The range gates of the Giraffe AMB radar system are about 50 meters. The longest pulse length used in the system is 64 sub-pulses, which gives us a smallest detection range to be approximately 3 kilometres.

3.3.2.2 Azimuth

To separate two targets in azimuth the targets should not interfere with each other, only clutter should be a source of error. The bearing distance between two adjacent targets must be at least half the target width; otherwise the simulated target radar-cross-section will be distorted, illustrated in Figure 13. In our case this means that the targets center is least at 4 degrees distance.

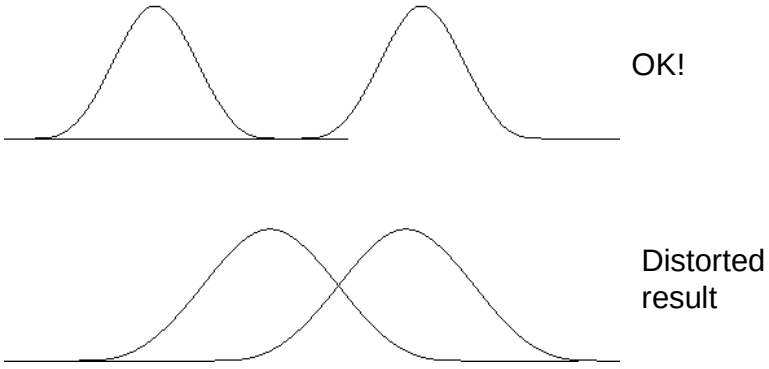

Figure 13 Truncation limit in azimuth

3.3.3 Result

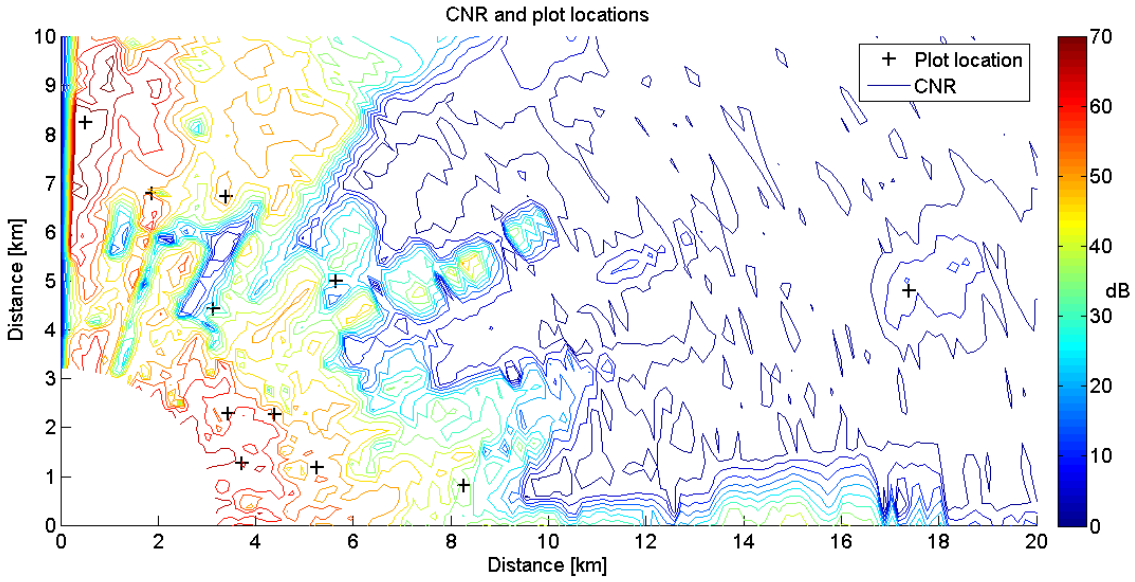

Figure 14 CNR map together with the plot locations.

The plots are positioned at different locations depending on the cell CNR. To decide where the plot should be place the averaging CNR map is used, which uses both transmission modes to estimated the CNR map. This will indeed introduce some false assumptions, as different radar settings will affect the clutter in different ways. The ideal case would be to sample video recordings from all the different transmission modes and system settings that is used in the measurements when gathering field data to the analysis.

3.4 Automatic measurement script

To assist in the process of measurements a script was designed, this was required as the measurements need to be logged at three different locations in the system and the measurements where too lengthy to be performed during office hours. The target simulator is connected to a controller built in MATLAB[3]. The controller defines the logging of data by a connection via TCP/IP to ERES (Extended Radar Evaluation System). ERES is Saab internal program used to evaluate radar data, it is connected to a Radar Control Unit (RCU) which can control the radar and set it to different modes, i.e. tx-mode, range and antenna revolution rate. The target simulator is connected to the signal processing unit interface (CISP).

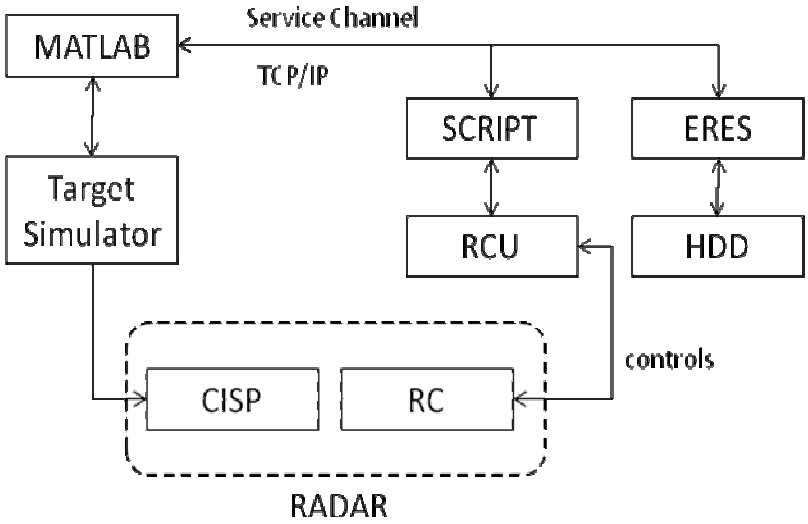

Figure 15 Schematic figure of the automatic measurement script

3.5 Plot association

For each target simulated the associated target detections are searched, the search volume to the simulated target position is 1 degrees in both azimuth directions, ±6 degrees in elevation and ±50 meters in range. If more than 80 % of simulated targets are found in the recordings that fulfil the requirements state above, a plot group is formed. I.e. if target is simulated at the same position and amplitude 30 times the plot group formed must have at least 24 detections within the same search volume. If there are several detections within the same revolution within a plot group the detection which are closest in elevation with respect to the simulated targets predicted elevation is selected. In addition the search window is moved in azimuth angle {±0.5, ±1, ±1.5, ±2} to find the plot group which contains most plots.

[3] MATLAB is a registered trademark of the Mathworks, Inc., Natick, Massachusetts, U.S.A.

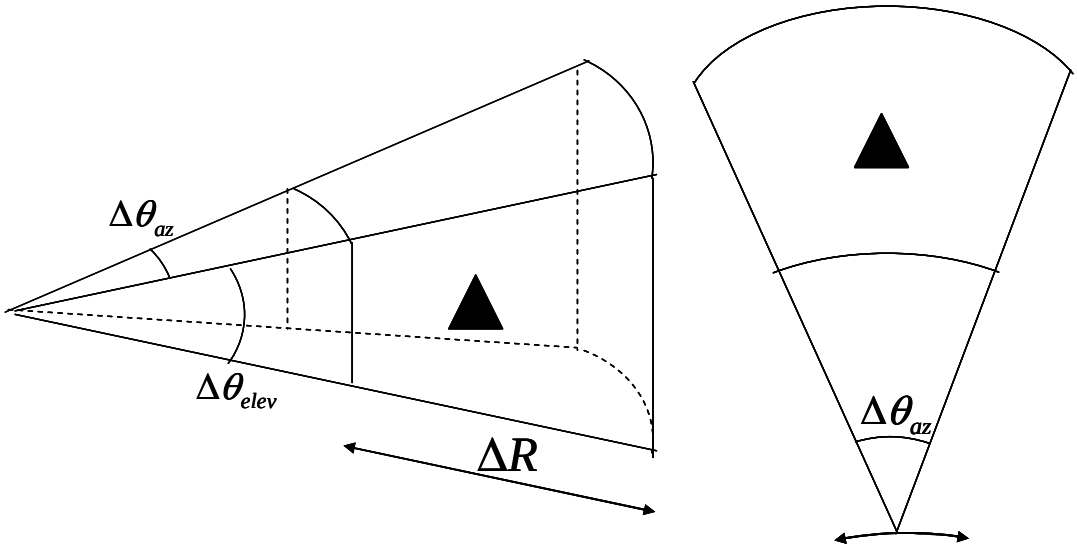

Figure 16 Search volume, the target is the small black triangle, the algorithm searches [-2,2]º azimuth to find the area most dense with targets.

To be able to analyse the result of the recorded measurements and be able to calculate (20), the measurement error, plot groups from the radar silence recordings and transmission recordings are associated. By doing so, a possible bias term between the plot position from the target simulator and the position from the radar system can be reduced. In the radar silence case no other signals then low thermal noise, which occurs in the receiver (Noise temperature) are present.

For two plot groups to be associated with each other the median bearing and elevation should be less than 1 degree from each other and the median distance should be less than 40 meters apart. It is therefore not necessary that a plot group found in the radar silence can be associated with a plot group in the transmission case. A reason for this could be that the clutter levels are so strong that the radar doesn't detect a low strength target; the target is simply drowned in the clutter or that the clutter scatters the target detections to a larger extent than what is allowed by the search algorithm.

3.5.1 RMS error

The Root Mean Square Error, RMSE (22) or Root Mean Square Deviation is calculated in azimuth, elevation and distance.

$$\varepsilon = \sqrt{\frac{\sum_i \left(\hat{x} - x_i\right)^2}{N}} \tag{22}$$

Where the sample mean from the non transmission recording is $\hat{x}$ and x_i is the sample value from the transmission recording and N is the number of samples in the current plot group. The non transmission or radar silence recordings are performed just to provide the correct position of the simulated target instead of calculating the relative error from the input parameters of the target simulator, thus, eliminating the independent error source.

The upper confidence bound for a sample standard deviation *s* is described by:

$$\sigma < \sqrt{\frac{(N-1)s^2}{\chi^2\left(\alpha/2, N-1\right)}} \tag{23}$$

Where, α is the confidence level.

As the measurement error is described by the sample standard deviation, and the data in a plot group is assumed to be normal distributed. A chi-square distribution is used calculated a 99.7 % confidence interval with N -1 degree of freedom, where N is the number of samples in the current plot group. A confidence interval must be calculated, so it is possible to be assure that the accuracy model doesn't overestimates the accuracy, with high probability.

3.6 Model requirements

As described in chapter 1.2 the model should be implementable in a real-time system with limited amount of processing power and time. The model should also never overestimate the accuracy as the tracker is more vulnerable to big changes when the accuracy is low.

Normally the tracker receives the estimated accuracy and decides a window that is three times larger than the given accuracy to be 99.7% confident that the target is within this window. In addition, it is important to have a smooth tracking feature, which is accomplished by having an approximately 20 % security marginal.

The two requirements are summarized:

1. $\overline{e_{measurement}} \approx \frac{\overline{\hat{e}_{measurement}}}{1.2}$, to get smooth tracking the mean estimated measurement error should be 20 % larger than the true mean error.

2. $\max(e_{measurment}) < 3 \cdot \hat{e}_{measurement}$, the maximum true measurement error should be less than three times the estimated measurement error, with a 99.7% confidence as described earlier.

3.7 Handling large scale errors

When predicting the elevation angle at least two different beams are needed. When one of the beams are missing a detection (for any reason) the radar system calculates the elevation angle based on the second highest amplitude from one of the two other beams. This leads to large elevation errors.

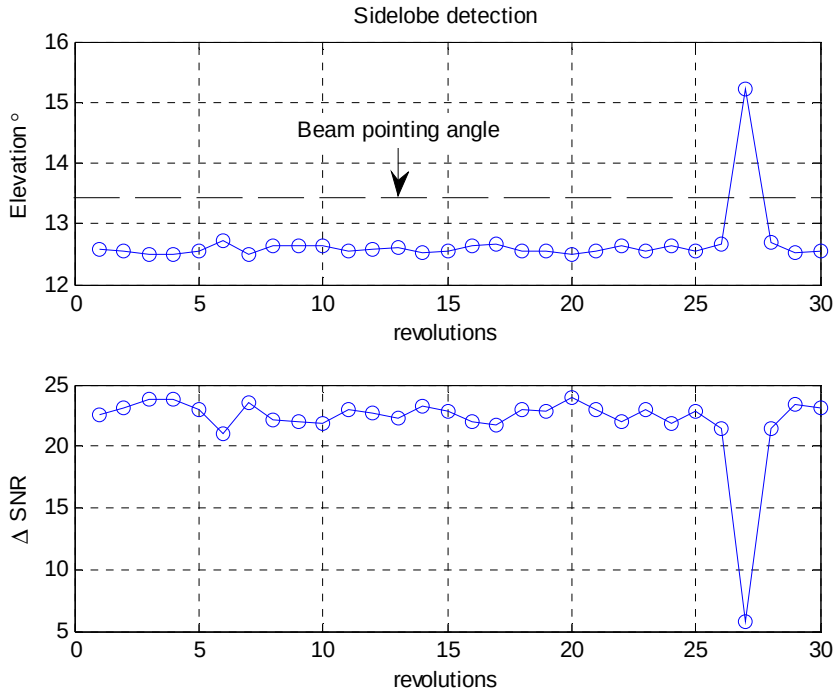

Figure 17 A case of large scale elevation error in a plot group, causing erroneous elevation estimation. Elevation beam pointing angle is dashed.

When clutter is strong in one elevation beam, the CFAR could remove the detection and thereby creating the large scale error which should not be capture by the linear curve fitting. Instead an outlier detector should capture this. Thus, when performing curve fit analysis this plots should be discarded, but the error should then be accounted for when outliers are analysed.

4 Result and analysis

After the plot association and plot group association a set of data is available which enables forming of the new accuracy model (24) by modification of (12). The data points are fitted to (18) using Least-Squares method based on elevation interval, amplitude, transmission type and coordinate, the resulting term is $\sigma_{AN,}$ angular error from noise or other random sources in equation below.

$$\sigma = \sqrt{\sigma_{AN}^2 + \sigma_{Outlier}^2} \tag{24}$$

The outlier error term is caused by radar system specific terms. The bias term from the (13) is disregarded, as this value is usually small.

A simple outlier model is proposed, which is defined with an amplitude criterion and an outlier contribution which is static over a specific interval. The outlier addition should be seen as the non-linear addition to the linear function to fully describe the measurement accuracy.

In the analysis 3σ is used to compare the algorithm towards other parameters and requirements. The use of three sigma is replaceable to for example four or five sigma; thus, changing how the performance indicators are produce does not change the result.

Verification is performed by using recorded GPS data from a real airplane together with the estimated position of the airplane from the radar system.

4.1 Target statistics

Target statistics describes the target statistics from the detections that are used in the analysis, they are important as the accuracy model is fitted to these target properties. The target statistics presented below are the RMS error calculated against the plot group mean for transmission recording in transmission mode A.

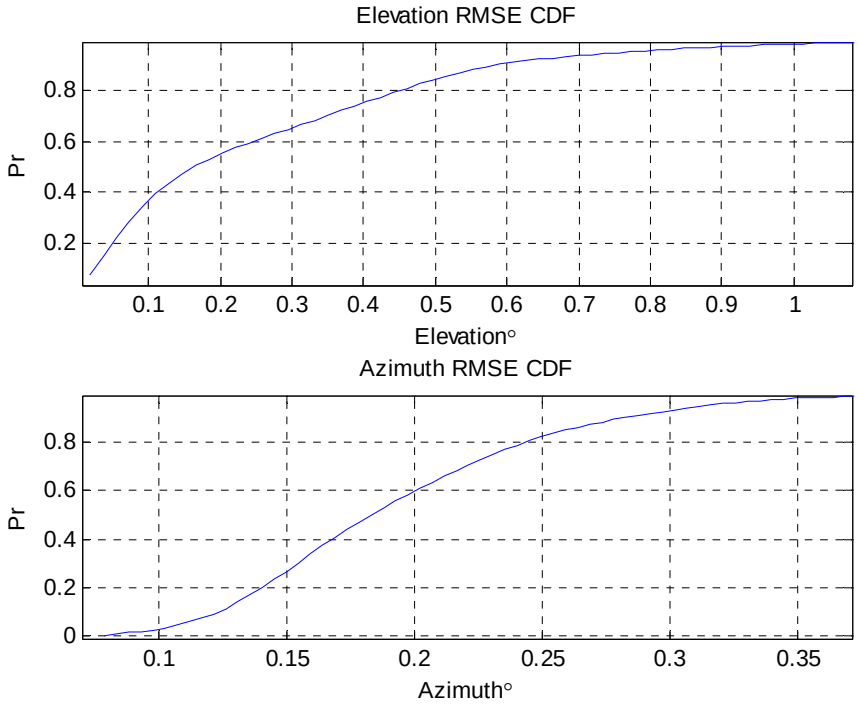

Figure 18 Root-Mean-Square-Error Cumulative Distribution Function for elevation and azimuth.

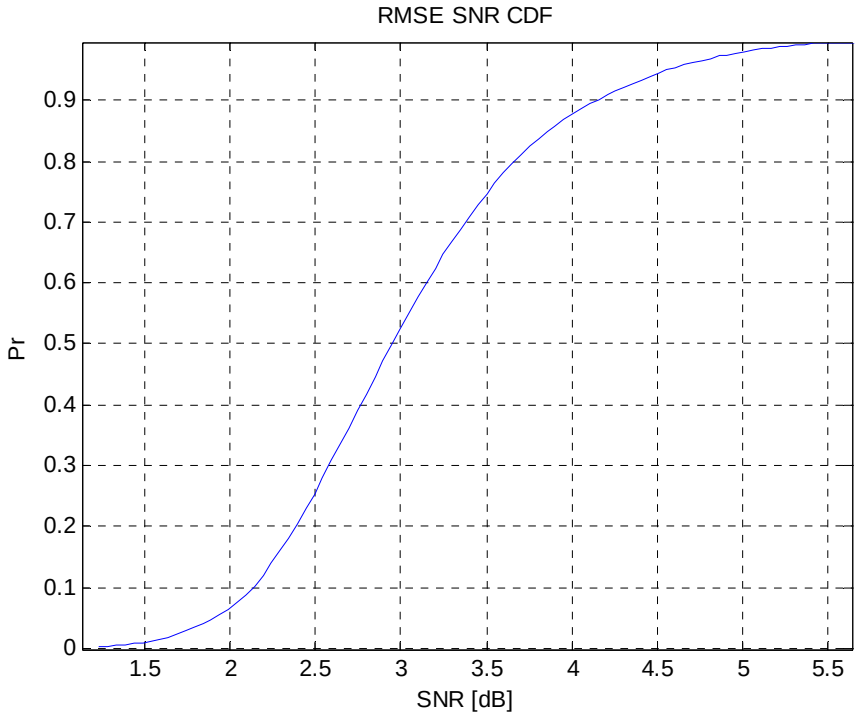

Figure 19 SNR Root-Mean-Square-Error Cumulative Distribution Function for plots in plot groups.

4.2 Elevation accuracy model

The model showed here are only for transmission mode A. The complete list of function parameters are provided in Appendix A.

The elevation accuracy model is divided into different elevation intervals, as the elevation accuracy is dependent on the elevation interval as shown in Figure 20, the mean elevation error differs between different elevation intervals. The intervals are chosen based on the receiving beams from the DBF, and statistical samples from the recorded data and manually adjusted.

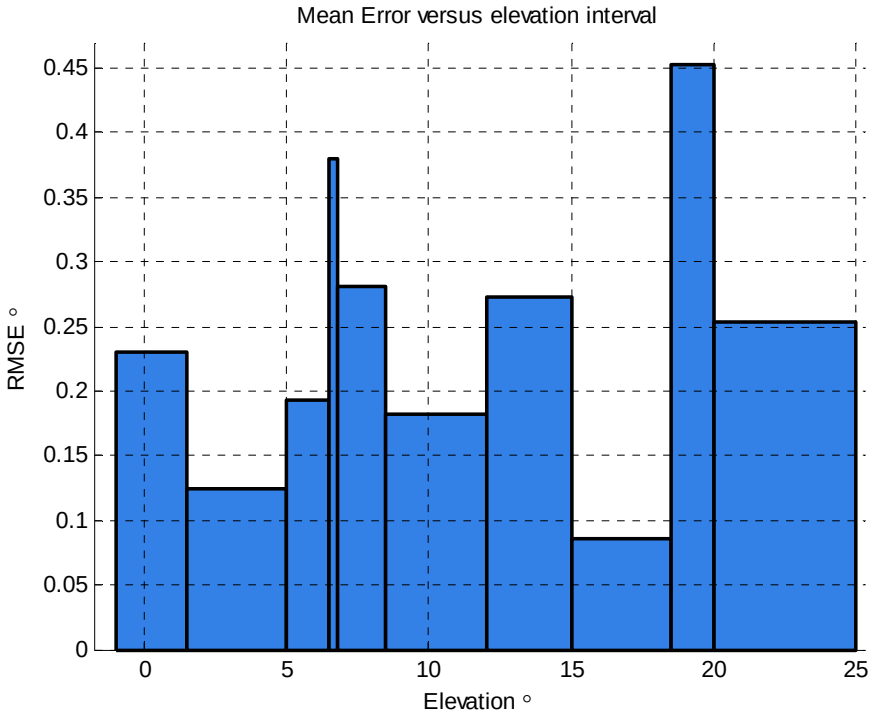

Figure 20 Elevation error dependence for elevation coordinates.

The data points are divided dependent on the elevation interval, a least-square fit to (9) is then made. To evaluate the fitted curve a filtering of the data is made, as can be seen in Figure 21 the fitted curve follows the filtered data points quite good. The most vital difference of the two curves is that the floor is a bit higher for the fitted curve and that the filtered data decays more slowly.

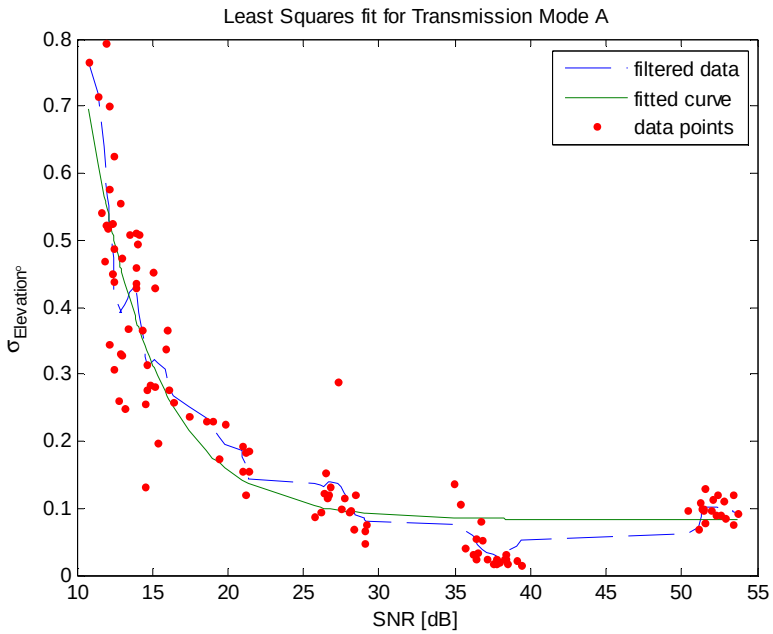

Figure 21 Least Squares fit for accuracy in elevation in Transmission Mode A, the detections is between -1 and 1.5 degrees elevation interval. A filtering of the data is made to visually evaluate the fitted curve.

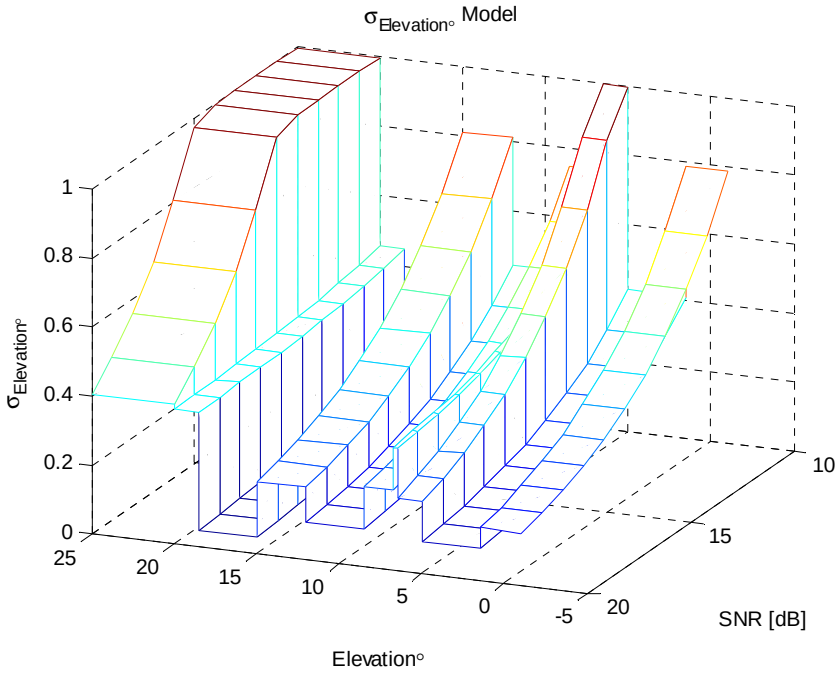

Figure 22 Accuracy model for Transmission mode A as a function of elevation and SNR, the model is limited at one degree to visualize.

The accuracy model is divided in SNR and elevation. As expected the model sets a lower accuracy for detections occurring in the beam pointing angles: 0, 7, 13 and 20. This can be the result of the effect when the target is not detected in one of the at least two elevation main beams that is demanded to make an accurate elevation estimation.

Transmission mode A is a low elevation system mode, with the highest elevation in 21 degrees and four receive beams are used. As the transmission mode has an upper limit, the elevations over the 4th beam pointing angle has a very bad performance value, the information from a second beam for elevation estimation is missing. Low amplitudes results in worse accuracy as expected, as clutter increases in low-angle regions and for low amplitudes as shown in this plot the accuracy will converge to half beamwidth as there will be less information in the closest beam to calculate the position, eventually, the target will only be detected in one beam.

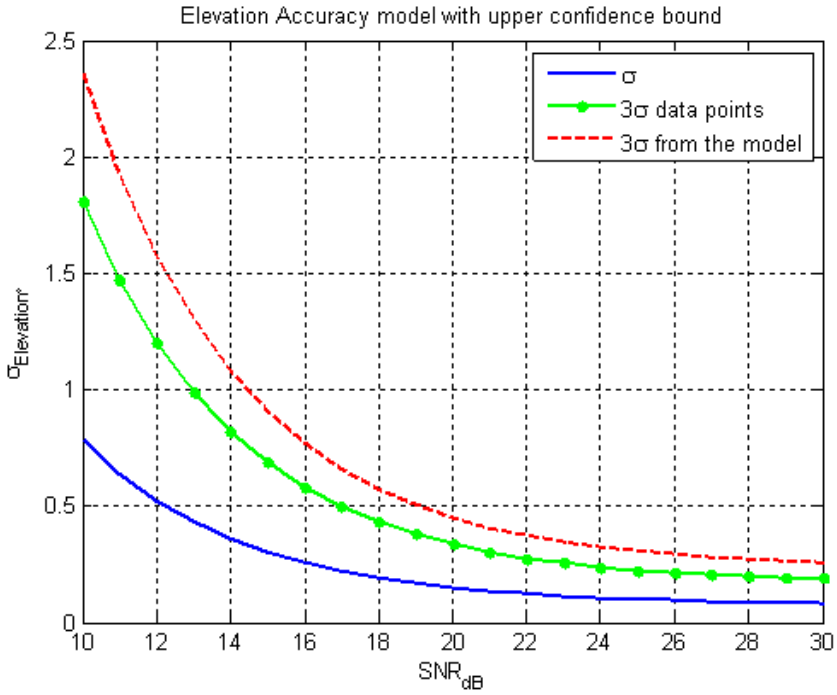

Figure 23 Elevation accuracy model for Transmission Mode A between -1° and 1.5°, 3 σ (99.73 %) upper confidence interval dotted, which is calculated by a new curve fit to the model using the upper confidence data points. The upper confidence bound that is calculated directly from the model (σ) is also plotted to visualize the difference between two methods for achieving an upper confidence bound.

4.3 Azimuth accuracy model

The azimuth model is found to be independent of the current elevation interval; therefore only one model is used. As the resolution in azimuth is higher than in elevation coordinate the error is much smaller. The upper confidence model is calculated by using Least-Squares, described earlier, to an upper confidence data set.

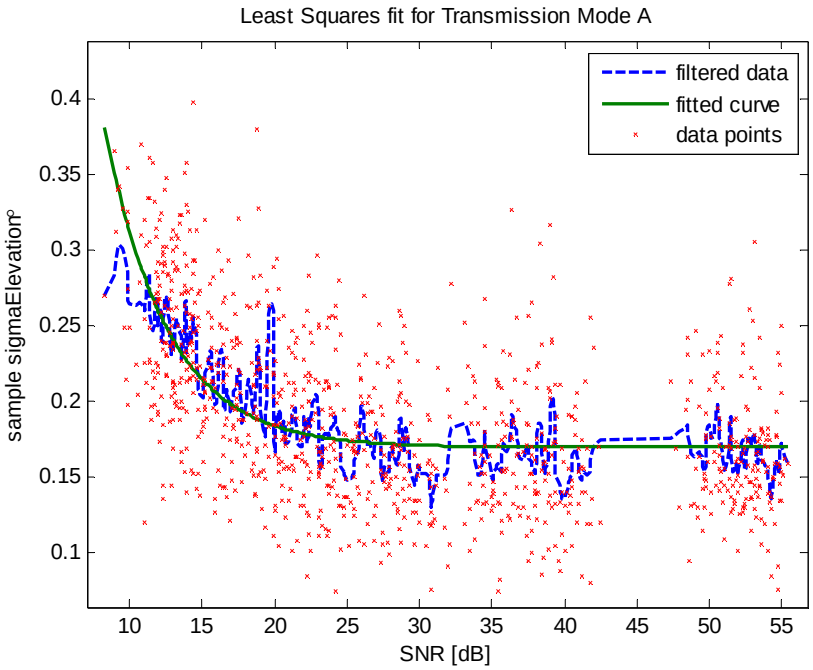

Figure 24 Least Squares fit for accuracy in azimuth, Transmission Mode A, for all detections. The filtered data is independent of the fitted curve and should be seen as an evaluation of correctness.

A 99.73% upper confidence bound is calculated according to (23), with the degrees of freedom determined by the number of plots in the current plot group.

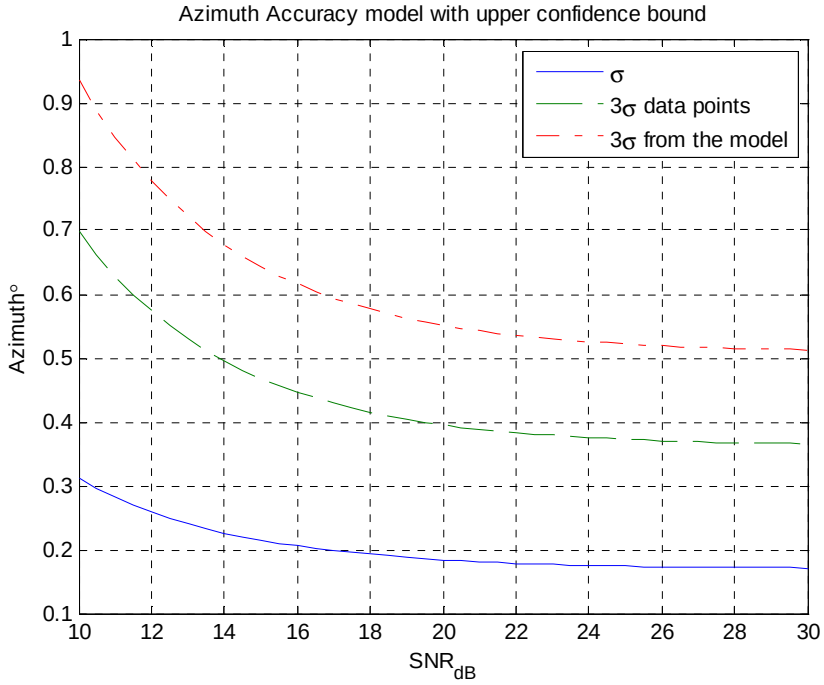

Figure 25 Azimuth accuracy model for Transmission Mode A, 3σ (99.73 %) upper confidence interval dotted. The upper confidence bound that is calculated directly from the model (σ) is also plotted to visualize the difference between two methods for achieving an upper confidence bound.

4.4 Outliers

One of the important things in this project is to find methods to detect when there is a high probability of outliers. It is important as the target tracking algorithm must be confident that the accuracy of a plot is correctly described. An outlier is defined as a detection which is larger than 3σ from the model.

Two steps are performed here:

1. Finding an outlier criterion and evaluate it.

2. Determine the outlier contribution.

In the measurements there are no outliers in azimuth coordinate, in the elevation coordinate the outliers are approximately 3 %. The outlier criterion is defined as: An outlier should be 50 % more probably to occur than a regular plot in the corresponding SNR interval. A ratio is the calculated to determine the range or bounds of the outlier criterion.

$$Ratio = \frac{\frac{\sum Outliers(SNR_i, SNR_j)}{\sum Outliers(SNR_{min}, SNR_{max})}}{\frac{\sum Regular(SNR_i, SNR_j)}{\sum Regular(SNR_{min}, SNR_{max})}} \quad (25)$$

Ratio calculation (25) determines where it is more probably to detect an outlier based on a SNR interval which starts at SNR_i and ends at SNR_j,each interval is 1 dB length. The functions: O*utliers* and *Regular* returns the amount of detections.

In Figure 26 the outlier's distribution normalized to the total number of detections as a function of SNR (25). The interpretation of this figure should be that, a value above one tells us that it is more probable that an outlier occurs than in an interval where the curve is below one. This means that the model is overestimating the accuracy for detections between approximately 20 to 40 dB and peaks at 23 dB, this can be because of a side-lobe detection if the side-lobe level is -23 dB related to the main beam/lobe . Based on these findings the outlier criteria can be designed.

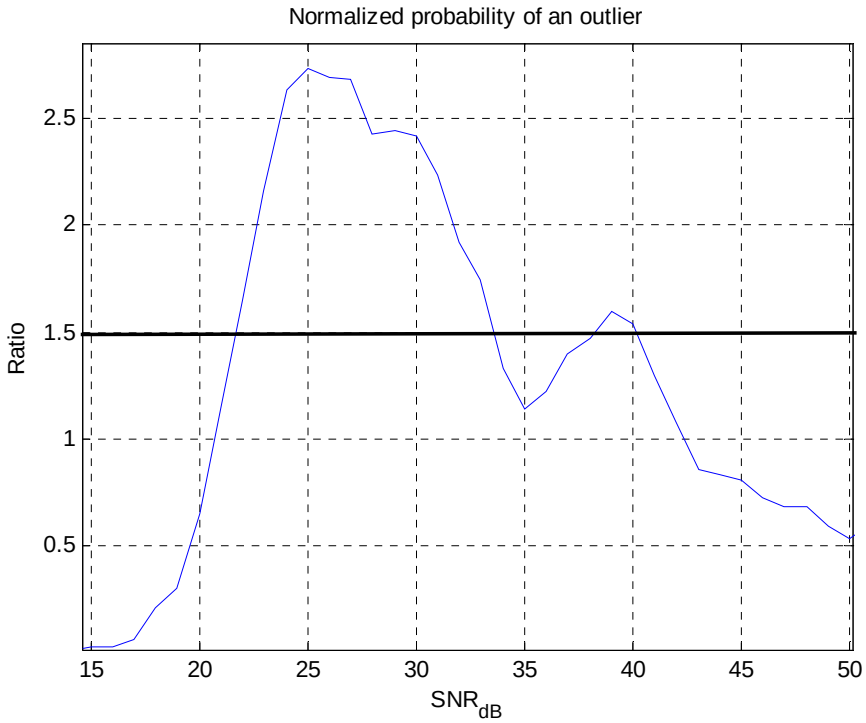

Figure 26 Distribution of outliers in elevation as a function of SNR, normalized to the total number of plots in corresponding SNR interval. A sum-filter with 5 dB length is used to smooth the curve. Values exceeding one are more probable to occur than values below. The dotted lines in the graph are showing the region where the plots are classified as outliers.

In elevation coordinate an outlier detector is formed if detection occurs between 21dB to 33 dB it is regarded as an outlier. To evaluate this principle two key numbers are identified in (26). The data points from the measurements in Transmission Mode A have ¼ of the plots in this interval and they will intersect with approximately 60 % of the total amount of outliers, so 60% is correctly classified as outliers. This means that about 40 % of the outliers are not regarded; they exist in other contexts, not capture by this model.

The amount of plots which are falsely classified as outliers is 23 % of the total amount of plots.

$$correctly\_classified = outliers \cap identified\_as\_outliers \tag{26}$$
$$falsely\_classified = (outliers \cup identified\_as\_outliers) - outliers$$

Figure 27 Azimuth and elevation outlier contribution CDF, in azimuth coordinate 90 % of the values are lower than 0.6° and in elevation coordinate 90% of the va lues are lower than 2.9°.

The outlier contribution tells us how much the addition in the accuracy model should be. For those plots that are classified as an outlier, either falsely or correctly, the value should be the 3σ model, e.g. Figure 21. In the elevation coordinate the contribution should then be ~1° and the highest possible accuracy should be set to $\theta_{3dB}/2$ which with a 3dB-beamwidth of 6.5° is 3.25°.

4.4.1 Outliers based on STR

For lower STR values the probability of an outlier is significantly higher, in the elevation model if it is 50 % more probable that an outlier occurs. This means that the CFAR algorithm has found a higher threshold in the surrounding cells, which indicates that the surroundings of the target are affected by clutter.

The CFAR algorithm produces a STR value between 0 and 6.12, approximately 68 % of the detections has a lower STR than 6.05. In Figure 28 the detections are quantized by 0.1 STR and a sum-filter of 0.5 STR length is used to smooth the curve. As over 30 % of the values are between 6.0 and 6.12, where small amounts of clutter exists, the accuracy is better than for lower STR values where the accuracy is worse as the clutter levels are higher.

In the recordings the amount of detections that is lower than 1.5 STR is extremely hard to find and therefore the analysis has not been projected in this area. Although, the observable trend is higher probability of an outlier, thus worse accuracy when the STR is decreasing, this is equivalent to a higher clutter value.

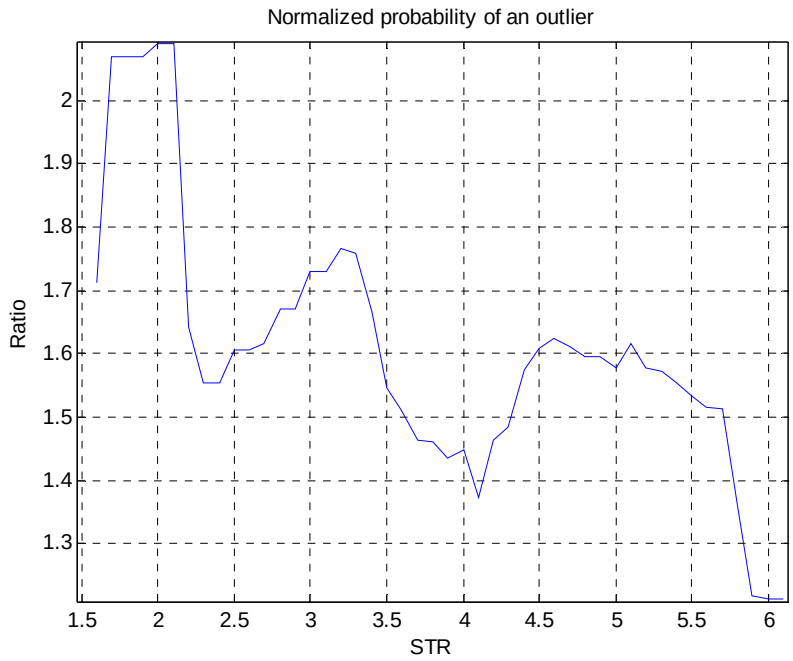

Figure 28 Normalized outliers to the total amount of outliers for elevation model, data is quantized in 0.1 STR intervals and a sum-filter with 0.5 STR lengths is used to smooth the curve.

4.5 Verification of accuracy model

The purpose of the verification is to determine if it is demanded to change any parameters of the model to fulfil the Model requirements described in chapter 3.6. The proposed model is the σ model.

To verify these criterions a real airplane with known position is used. From the radar origin perspective, the airplane starts at 6 degrees elevation aspect angle, goes down to 1 degree and returns to 6 degree. In distance it travels 100 km, starting at 10km turning at 60km and returns to the origin. The flight occupies a 45 degree sector, the flight time is 22 minutes and the average velocity is 75 m/s. The model used is for Transmission mode A as the flight recording is made with the same transmission mode and the position error is neglected.

It should be noticed that the environment where the verification is done is not the same as the environment where the recordings are made. This implies that the clutter environment differs from the clutter environment used when designing the accuracy model algorithm, as the algorithm should function in all types of clutter environment, the algorithm should function in this environment as well.

4.5.1 Elevation

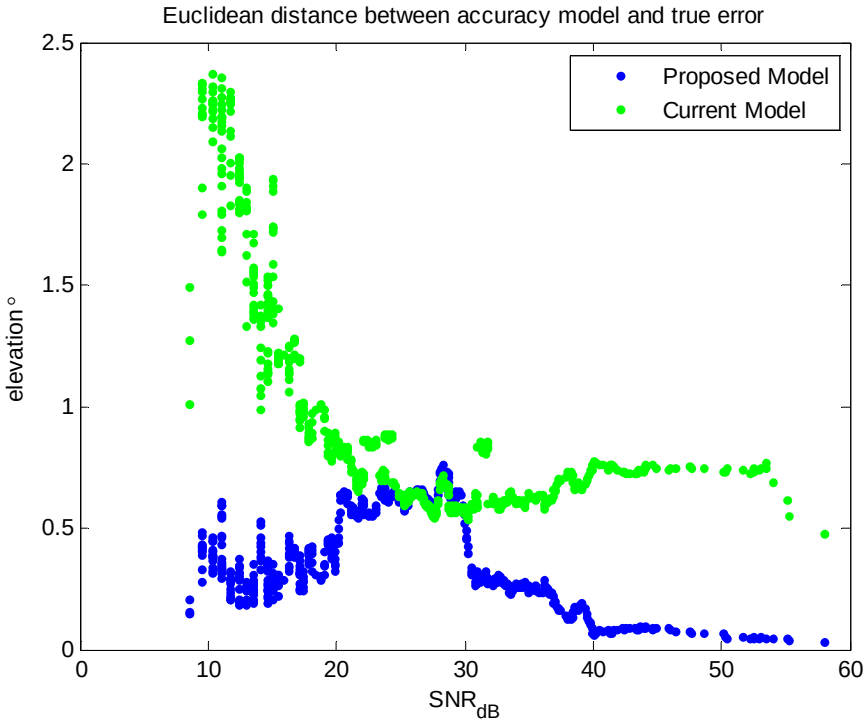

Figure 29 Euclidean distance (absolute value) between true accuracy and current model as well as the proposed model. It is shown that the proposed model follows the true error better than the current model, as the proposed model has a smaller distance from the true error compared to the current model.

Without outlier compensation the proposed model has 0.28 degrees mean deviation from the true error, but then the model requirements are not fulfilled. With an outlier compensation of 1 degree in the interval between 21 dB and 33 dB, a multiplication constant that is determined for this case, a unison floor raise and a compensation depending on the current elevation interval the final accuracy model is described in (27), the mean error is 0.43 degrees. This is compared to the current model which has a mean error of one degree. The main difference between the models is that the low amplitudes intervals are treated much more accurate than the current model and elevation dependent accuracy.

The final accuracy model in elevation is:

$$\sigma_{final\_model} = \begin{cases} \sqrt{(1.2\sigma)^2 + 1}, SNR = [21,33]dB \\ \begin{cases} \sqrt{(1.2\sigma)^2 + 0.45^2}, Elevation > 5° \\ \sqrt{((1.2 \cdot 1.3)\sigma)^2 + (0.45 \cdot 1.3)^2}, Elevation < 5° \end{cases}, SNR \neq [21,33]dB \end{cases} \quad (27)$$

By differentiating the floor and the multiplication constant based on the corresponding elevation interval is possible as earlier described in Figure 20, the magnitude of the error is dependent on the elevation interval. For this verification the target elevation was only between 1.5 to 5 degrees and between 5 to 6.5 degrees and 10 % of the values where in the higher elevation interval. The result here is only valid for elevations up to 6.5 degrees and should be extended to cover the full elevation coverage.

Summing the current model and the proposed models errors to the true error shows a 7 times improvement for the proposed model, then both models applies to the two requirements. Note, that approximately 0.3 % of the largest errors are removed from this verification as the model should have a 99.7 % probability of correctness. Errors that are larger than half-beam width are also removed, as they are considered to be caused by other effects than clutter.

Further fine-tuning might improve the result, although the fine-tuning should be verified at different measurement sites in order to verify its correctness.

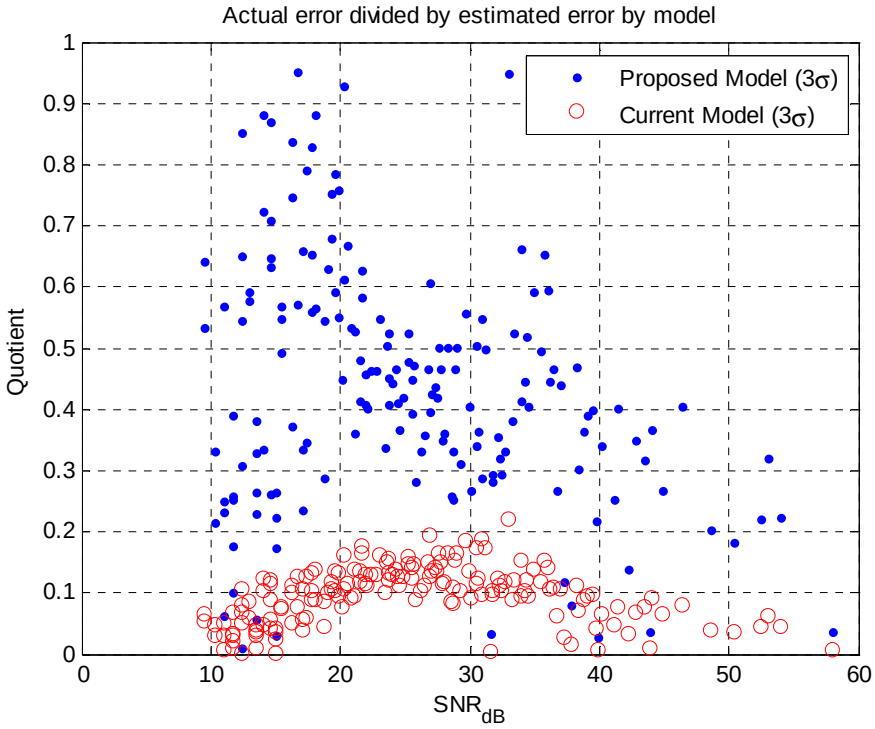

Figure 30 Quotient between the actual error and the estimated error from the 3σ model. A value above one indicates that the estimated accuracy is overoptimistic, a value below one is wanted. Plots are randomly chosen to illustrate the quotient.

The quotient of true error and estimated error is described in (28). This quotient should never exceed one for the first requirement to be fulfilled.

$$Quotient = \frac{true\_error}{3\sigma} \tag{28}$$

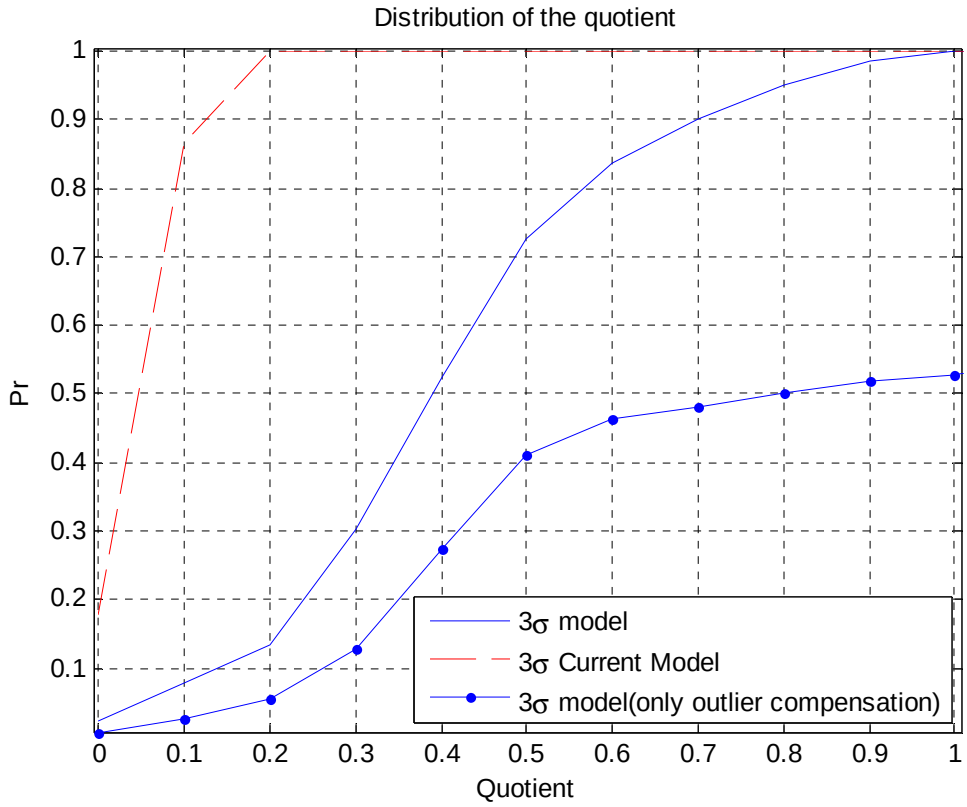

Figure 31 Distribution of the quotient after applying (27), when only applying the outlier compensation and the current model. The optimal estimation should be close to the true error, thus the quotient should be equal to one at all times.

The quotient should in the ideal case be one for all values, but as this is not practical achievable as this would mean the estimated accuracy is always same as the true error. Instead the focus should be to minimize the low quotients as far as possible, when only applying outlier correction to the curve; the model overestimates over 50 % of the plots. The benefit of using a method described by (28) is the distance between the quotient for the current model and the 3σ model.

The improvement factor in terms of RMS error is in the σ domain 0.5 and in the 3σ 8.4, this is caused by that optimization is done towards the first model requirement. Thus, a lot of detections are overestimated in σ domain, but they are not overestimated in 3σ domain. The second requirement are not fulfilled as the mean estimated error is two times larger than the true error. But this is not essential as the estimated error is larger than the true error.

4.5.2 Azimuth

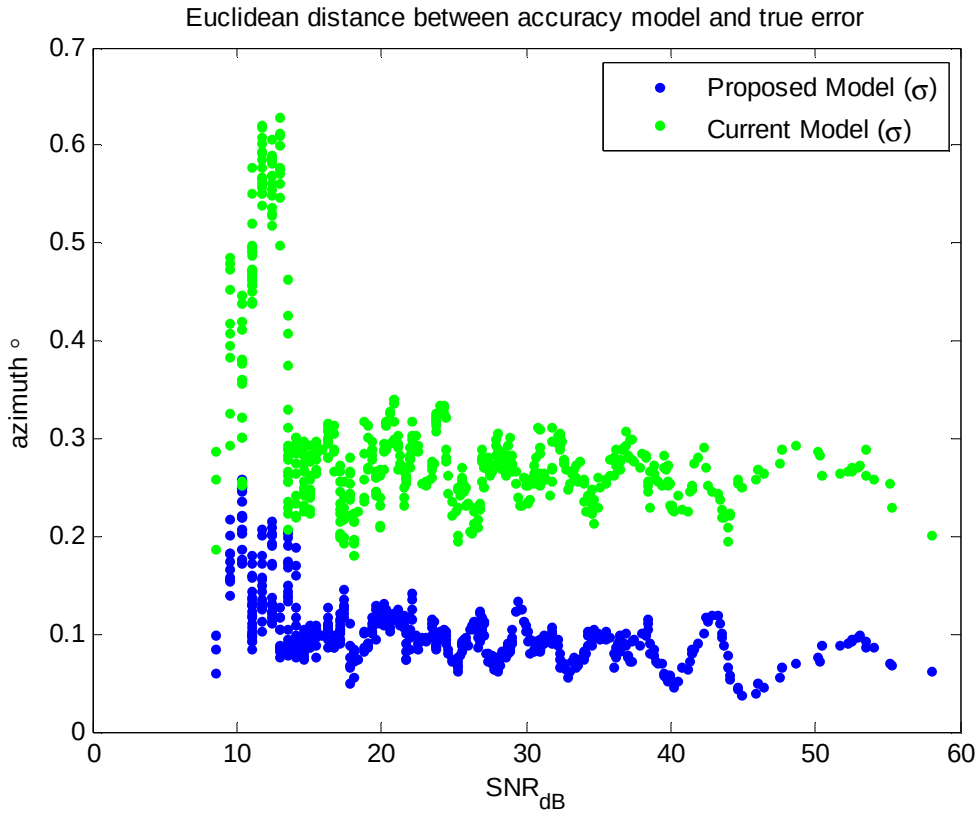

Figure 32 Euclidean distances between true accuracy and current model as well as the proposed model. It is shown that the proposed model follows the true error better than the current model as the Euclidian distance is smaller.

The current models mean deviation from the true error is approximately 0.32 degrees, while the proposed model mean deviation is 0.10 degrees. The proposed model is therefore three times tighter than the current model implementation.

In the verification process a few percentages of the data from the recordings has azimuth errors larger than the beamwidth, this is likely caused by mistakes made in the tracker or some unknown source of error in the radar system and is removed from the validation. None of the models are overestimating the accuracy, thus the proposed model applies to first requirement. The second requirement are fulfilled exactly.

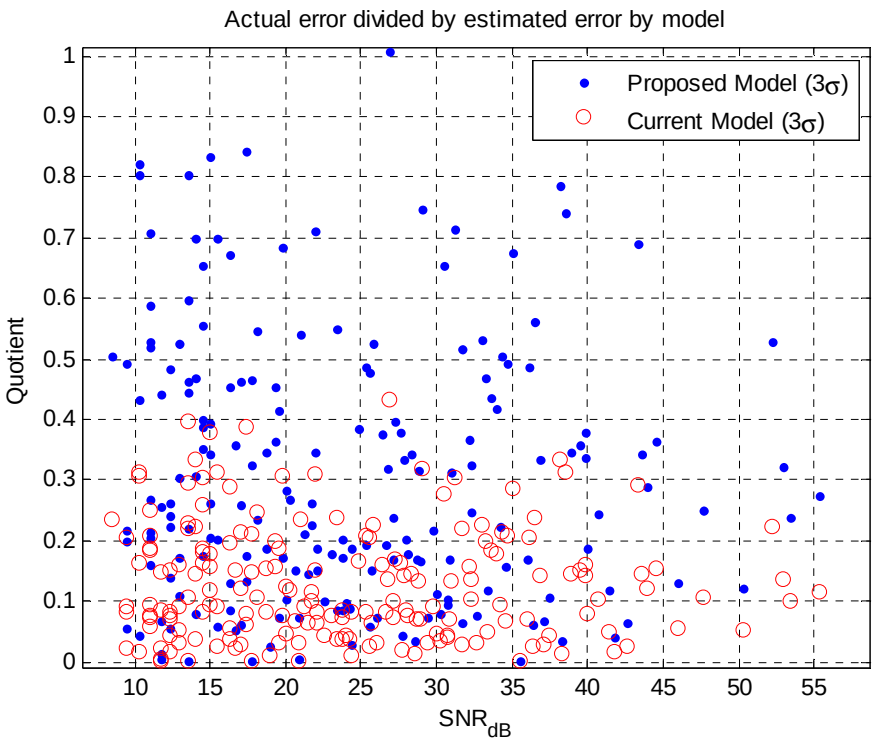

Figure 33 Quotient between the actual error and the estimated error from the 3σ model. A value above one indicates that the estimated accuracy is overoptimistic; a value below one is wanted. 30 % of the detections are randomly chosen.

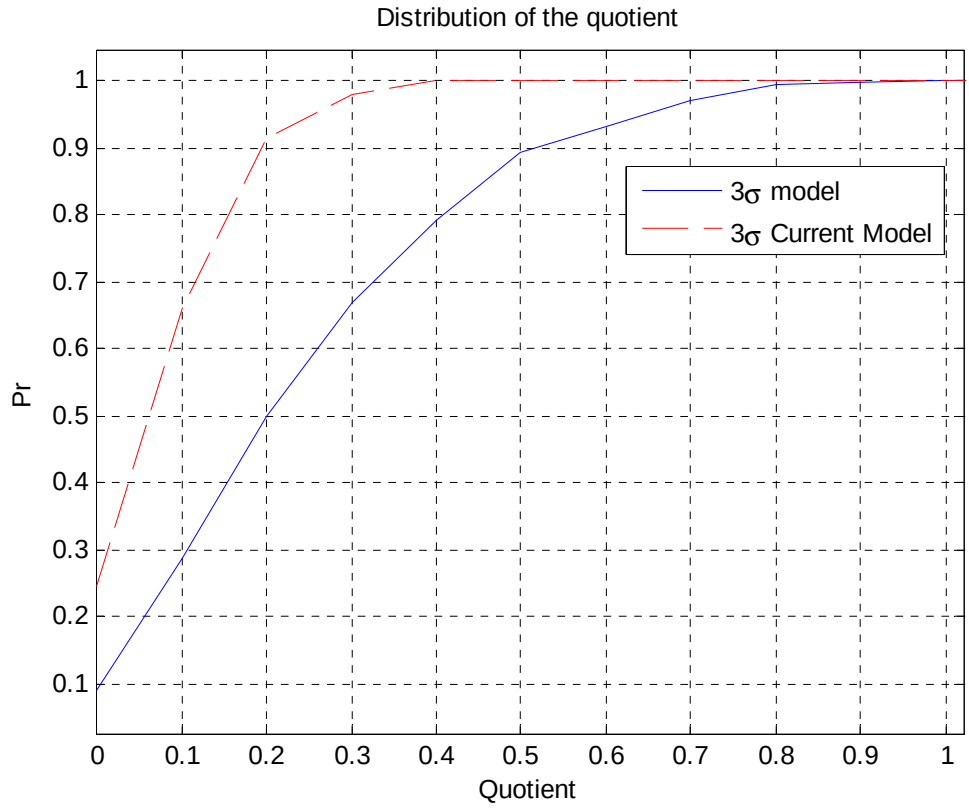

Figure 34 Distribution of the Quotient presented in Figure 33. It's obvious that the models don't differ much.

4.6 Verification of recordings

Two measurements where done, one measurement that included the STR values where unusable because of an error in the connection between the simulator equipment and radar interface.

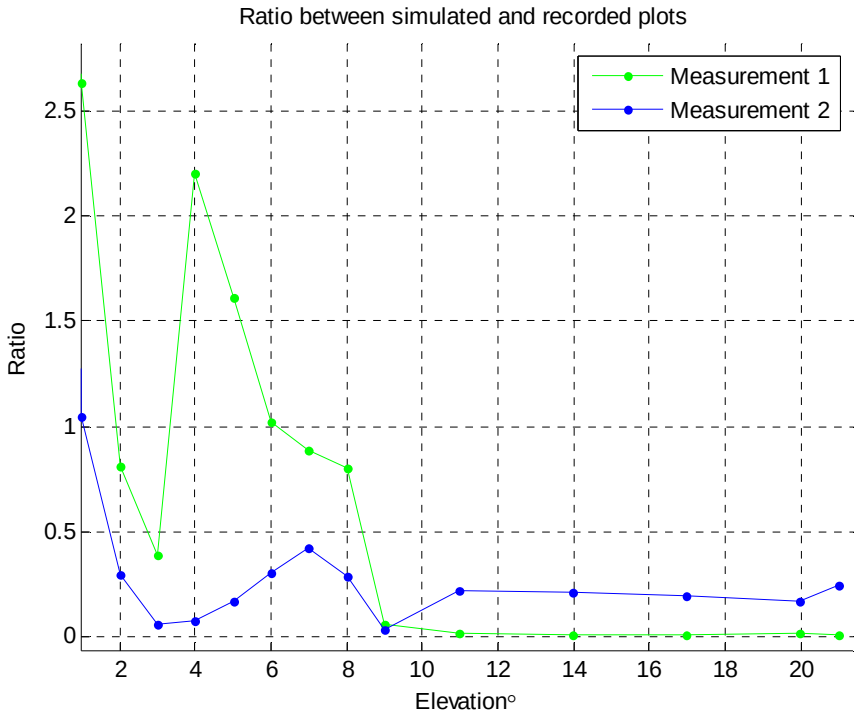

Figure 35 Ratio received plots in elevation to simulated plots in elevation. The elevations numbered on the x-axis are the simulated targets pattern. The ratio should in the ideal case be one. It should be noticed that the elevations simulated are: [0,1,2,3,4,5,6,7,8,9,11,14,17,20] as found in Table 6.

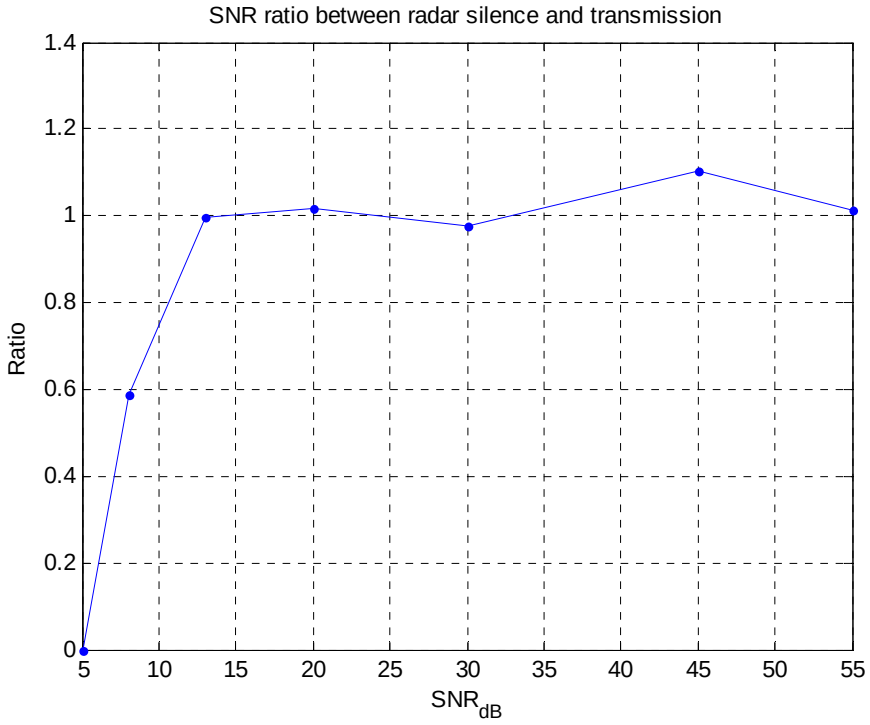

Figure 36 Target amplitude distribution for transmission mode A. In the ideal case the relation should be one, which means that the simulated targets and the detected targets has equal ratio.

Target amplitude distribution should in the ideal case be uniform, as can be seen from Figure 36 low amplitudes are hard to detect as a consequence of the limited radar sensitivity. A value above one in Figure 36 does mean that the ratio of the detected plots is higher than the ratio of a simulated plot in the same interval. This means that about 10 % of the plots in the 45 dB interval are garbage, however this is not crucial as the other points are below one or one and the 45 dB interval will only affect the floor of the model. This could be the cause of the lower accuracy in Figure 21's 45 dB interval, but it could also be caused by a fixed random error which degrades the accuracy in higher SNR intervals as described in Ch. 2.1.4 Measurement Accuracy.

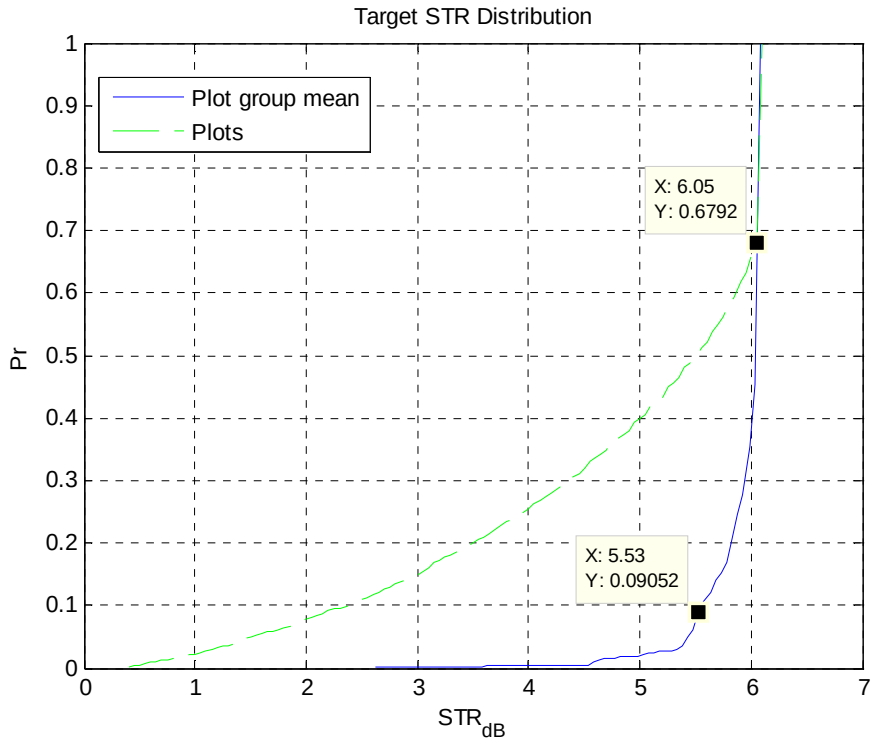

Figure 37 STR distribution for single plots and plot group means.

The problem of finding STR values at a lower interval is illustrated in Figure 37, 68 % of the STR values are lower than 6.05, the highest possible STR value is 6.1. This shows that about 30 % of the data has no or very little impact from clutter sources. For the plot groups a mean can be formed and the result shows that 10 % of the plot groups mean is lower than 5.5 STR, which limits the possibility of an analysis of the data.

4.6.1 Bias

In the recordings a small bias is produced at elevation coordinate, the bias are directed to zero degrees elevation and is therefore likely to be caused by ground clutter. The bias error in elevation is in 60 percent of the cases zero degrees, only a small higher bias error is noted as the effect from ground clutter. The bias error is usually small compared to the model error.

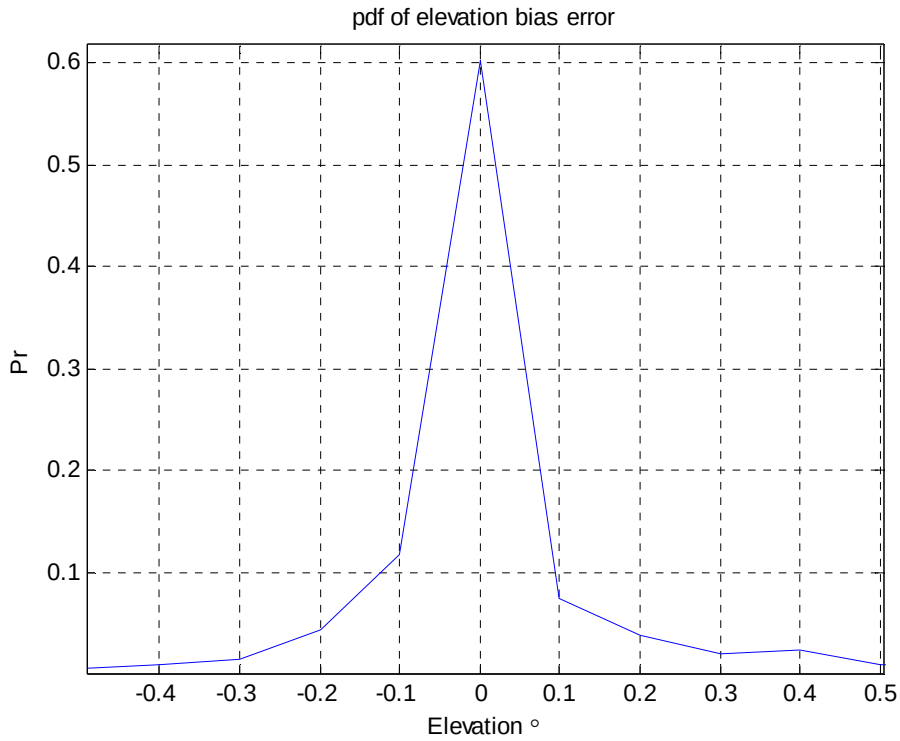

Figure 38 Probability Density Function of the bias error in elevation.

4.6.2 Plot association

Overall a simulated plot in a measurement series has 42 % probability to be detected and associated with a plot group in radar silence and 30 % probability with radar transmission. For Transmission Mode A the total numbers of detections that are used in the calculations are approximately 30,000 in the transmission recordings and 15,000 in the radar silence case. In azimuth the whole revolution (360°) is used up to 3 0 km range in a 20 degree elevation interval. The recordings took approximately 1 hour to perform plus an additional half hour for the recordings in the non transmission case. In total 1100 plot groups are formed.

5 Conclusions

The accuracy measured corresponds to the theoretical accuracy as a function of SNR. The contribution is that the new model treats each elevation interval in elevation coordinate as a separate accuracy model. The new accuracy relationship has shown that the accuracy is lower for detections in lower elevations and for detections near the beam pointing angle in the elevation coordinate.

During a test scenario with a real airplane flying a low elevation trajectory the proposed model is 7 times tighter than the current model in elevation coordinate when no overestimations are required. In azimuth the proposed model is 1.1 times tighter than current model with no overestimations. The performance value could be better if the raise in the floor could be adjusted for different elevation intervals; this is only applicable in the elevation coordinate.

The current model in azimuth coordinate has showed to be accurate, without any adjustments the accuracy for the azimuth accuracy estimation could be improved by 300%.

The concept of using STR as an indicator of accuracy is not completely satisfactory; the environment used is not as clutter dependent as predicted. A higher statistical certainty with low STR values is needed. Although, the trend with STR and accuracy has been illustrated, based on those results provided in this paper a precautionary proposal is that lower STR than the maximum STR allowed, as STR is limited, should set the accuracy to half the beamwidth which is the worst accuracy.

6 Further work

The simulations do not include simulation of multipath effects, target multipath echoes is often a critical factor which will degrade the radar performance. It's shown in several papers that that the multipath echoes will largely depend on the illumination angle and the terrain backscattering. Thus, this implies that to investigate the accuracy relationship a study with real targets or a model including multipath properties needs to be performed.

Further investigation also needs to be made with the concept of error dependence as a function of STR.

Transmission mode A is only evaluated and verified in this paper, a complete analysis should include all different types of transmission modes available in the system. This has to be done if the accuracy estimations could be implemented in a real radar system.

The verification was done with one trajectory and one airplane in one environment. Thus, to fully evaluate and verify the proposed accuracy model different airplanes and different environments should be tested.

7 References

[1]. **Barton, D. K.** *Radar system analysis and modeling.* Boston, Mass : Artech House, 2005. ISBN 1580536816.

[2]. **Miller, S. Childers, D.** *Probability and Random Processes: With Applications to Signal Processing and Communications.* s.l. : Academic Press, 2004. ISBN 0121726517.

[3]. **Billingsley, J. Barrie.** *Low angle radar land clutter.* Norwich, N.Y. : William Andrew Pub., 2002. ISBN 1591242371.

[4]. **Skolnik., Merrill I.** *Radar Handbook.* New York : McGraw-Hill, 1990. ISBN 1591244803.

[5]. **Stimson, G. W.** *Introduction to Airborne Radar.* 2 ed. Mendham, N.J. : SciTech Pub., 1998. ISBN 1891121014.

[6]. **Curry, Richard G.** *Radar system performance modeling.* Boston, Mass. : Artech House, 2005. ISBN 1-58053-816-9.

[7]. **Volakis, J. L.** *Antenna engineering handbook.* 4 ed. New York : McGraw-Hill, 2007. ISBN 0071475745.

[8]. **Barton, D. K.** *Handbook of Radar Measurements.* Dedham, MA : Artech House, 1984.

[9]. *Classification of radar clutter in an air traffic control environment.* **Haykin, S. et al.** June 1990, Proceedings of the IEEE, pp. 742-772.

8 Abbreviations

AMB	- Agile Multiple Beam
CFAR	- Constant False Alarm Rate
CISP	- Customer Interface Signal Processing
CNR	- Clutter-To-Noise Ratio
ERES	- Extended Radar Evaluation System
HDD	- Harddisk
PRF	- Pulse Repetition Frequency
PRI	- Pulse Repetition Interval
Plot	- A target detection
RC	- Radar Control
RCU	- Radar Control Unit
RMS(E)	- Root-Mean-Square (-Error)
RSS	- Root-Sum-Squares
STR	- Signal-To-Threshold Ratio
SNR	- Signal-To-Noise Ratio
TCP/IP	- Transport Control Protocol / Internet Protocol
TWT	- Travelling Wave Tube